

Review

Bacteriorhodopsin: a high-resolution structural view of vectorial proton transport

Richard Neutze^a, Eva Pebay-Peyroula^b, Karl Edman^a, Antoine Royant^{b,c},
Javier Navarro^d, Ehud M. Landau^{d,*}

^aDepartment of Molecular Biotechnology, Chalmers University of Technology, Box 462, S-40530 Göteborg, Sweden

^bInstitut de Biologie Structurale, UMR5075, CEA-CNRS, Université Joseph Fourier, 41 rue Jules Horowitz, F-38027 Grenoble Cedex 1, France

^cEuropean Synchrotron Radiation Facility, 6 rue Jules Horowitz, BP 220, F-38043 Grenoble Cedex, France

^dMembrane Protein Laboratory, Department of Physiology and Biophysics, Sealy Centers for Structural Biology and Molecular Science, The University of Texas Medical Branch, 301 University Boulevard, Galveston, TX 77555-0437, USA

Received 16 January 2002; accepted 30 July 2002

Abstract

Recent 3-D structures of several intermediates in the photocycle of bacteriorhodopsin (bR) provide a detailed structural picture of this molecular proton pump in action. In this review, we describe the sequence of conformational changes of bR following the photoisomerization of its all-*trans* retinal chromophore, which is covalently bound via a protonated Schiff base to Lys216 in helix G, to a 13-*cis* configuration. The initial changes are localized near the protein's active site and a key water molecule is disordered. This water molecule serves as a keystone for the ground state of bR since, within the framework of the complex counter ion, it is important both for stabilizing the structure of the extracellular half of the protein, and for maintaining the high pK_a of the Schiff base (the primary proton donor) and the low pK_a of Asp85 (the primary proton acceptor). Subsequent structural rearrangements propagate out from the active site towards the extracellular half of the protein, with a local flex of helix C exaggerating an early movement of Asp85 towards the Schiff base, thereby facilitating proton transfer between these two groups. Other coupled rearrangements indicate the mechanism of proton release to the extracellular medium. On the cytoplasmic half of the protein, a local unwinding of helix G near the backbone of Lys216 provides sites for water molecules to order and define a pathway for the reprotonation of the Schiff base from Asp96 later in the photocycle. A steric clash of the photoisomerized retinal with Trp182 in helix F drives an outward tilt of the cytoplasmic half of this helix, opening the proton transport channel and enabling a proton to be taken up from the cytoplasm. Although bR is the first integral membrane protein to have its catalytic mechanism structurally characterized in detail, several key results were anticipated in advance of the structural model and the general framework for vectorial proton transport has, by and large, been preserved.

© 2002 Elsevier Science B.V. All rights reserved.

Keywords: Bacteriorhodopsin; Energy transduction; Kinetic crystallography; Proton pumping; Structural mechanism

1. Introduction

Vectorial ion transport across a cell membrane is a beautiful and ubiquitous function in biology. Proton pumping lies at the heart of Mitchell's theory [1] of chemiosmotic coupling, whereby light [2] or electrochemical energy [3,4]

is first converted into a proton-motive potential by a chain of integral membrane proton pumps [5], and the energy thus stored within this potential is harvested by ATP synthase [6] so as to regenerate ATP from ADP and Pi. The continuous regeneration of a proton-motive potential thus displaces the $ATP \leftrightarrow ADP + Pi$ equilibrium approximately 10 orders of magnitude from equilibrium and the excess of ATP acts as the basic energy currency of the cell. X-ray structures of the calcium pump Ca^{2+} -ATPase [7] and the light-driven chloride pump halorhodopsin (hR) [8] provide a structural basis for understanding how cation and anion concentrations are controlled within the cell using very different sources of energy.

Abbreviations: bR, bacteriorhodopsin; hR, halorhodopsin; SR, sensory rhodopsin; O.D., optical density; FTIR, Fourier transform infrared; LT, Low temperature; σ , root mean square electron density

* Corresponding author. Tel.: +1-409-772-8635; fax: +1-409-772-1301.

E-mail address: emlandau@utmb.edu (E.M. Landau).

Bacteriorhodopsin (bR) is the simplest known light-driven proton pump. This small integral membrane protein belongs to the family of archaeal rhodopsins, all of which exhibit a heptahelical transmembrane architecture, and contain a buried retinal chromophore covalently bound to a conserved lysine residue in helix G via a protonated Schiff base. Although first discovered within halophilic archaeobacteria [9,10], related rhodopsins were later identified in eubacteria [11] and unicellular eukaryotes [12]. In addition to bR, the family of archaeal rhodopsins include hR, which harvests light so as to pump chloride ions from the extracellular medium into the cytoplasm [13], and two sensory rhodopsins (SRI and SRII) [14] which mediate positive or negative phototaxis in the host archaea in response to changing environmental conditions. All archaeal rhodopsins undergo a series of light-induced reactions, called a photocycle, the primary event of which is the photoisomerization of the all-*trans* retinal chromophore to the 13-*cis* configuration. Despite their functional diversity, it has often been suggested that a common mechanism of action is manifest within the family of archaeal rhodopsins [13,14]. This idea is further emphasized by the observation that under certain conditions, ion selectivity and vectoriality may be reversed [13]. Nevertheless, at a detailed molecular level, subtle yet significant differences are to be expected.

Due to bR's simplicity and stability, and to the fact that bR is highly enriched in the native membrane, it has long served as the prototype for elucidating general features of vectorial ion transport across a cell membrane. An enormous body of biophysical knowledge deriving from a plethora of biochemical, genetic and spectroscopic investigations has been built up over the three decades since bR was first identified as a proton pump [10]. Three-dimensional structures of bR at increasing resolutions [15–18] reveal the positions of a number of charged residues and water molecules arranged to form the proton translocation channel that extends across the membrane through the center of the heptahelical bundle. Light-induced structural changes cause these residues and water molecules to act as if members of a relay team, passing a proton from one group to another in a well-orchestrated sequence of events (Fig. 1) which have been characterized through detailed spectroscopic and mutational studies (for a succinct review see, e.g. Ref. [19]). As such structural rearrangements of the protein serve both to define a pathway for proton exchange between charged groups for each step of this process, and to manipulate the pK_a 's of the key residues so that the correct proton donor/acceptor relationship is achieved at the required point in the photocycle. The remarkable fact that light-induced structural rearrangements are able to both switch the accessibility of the Schiff base, and to reverse its proton donor/acceptor relationship with respect to key charged groups, is the essence of vectorial proton transport in bR.

This reaction sequence in the bR photocycle is summarized in Figs. 1 and 2. Light energy is first absorbed by bR

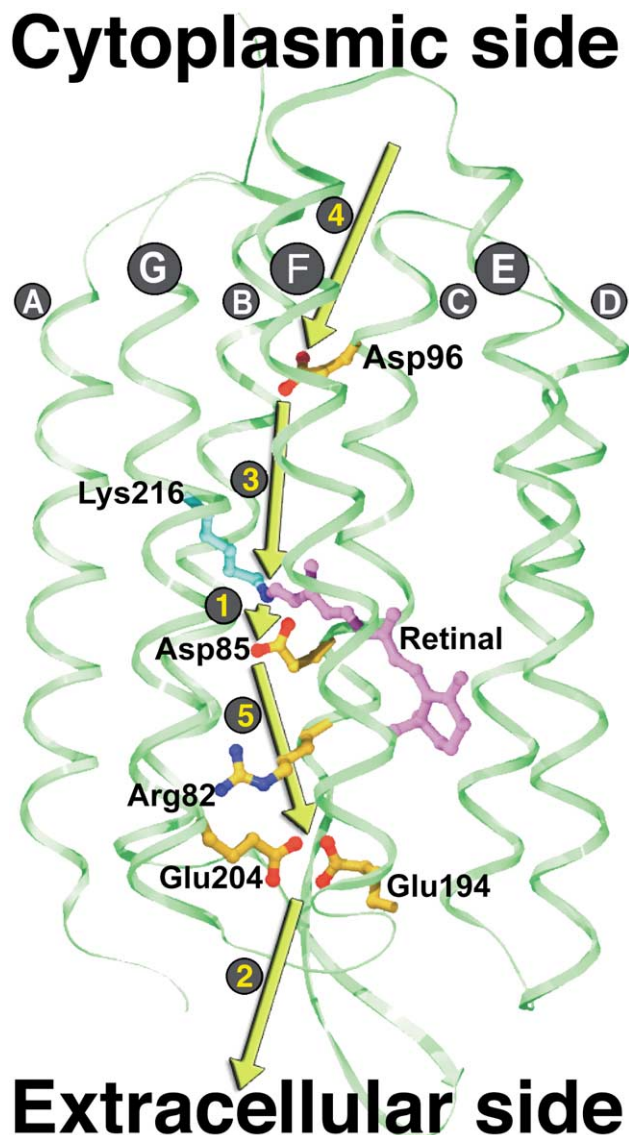


Fig. 1. Schematic representation of the proton transfer steps in the bR photocycle, overlaid on the ground state model (ribbon representation in green, showing helices A to G). Strategic residues that participate in the proton transfer (Asp96, Asp85, Arg82, Glu194, Glu204), as well as the retinal bound to Lys216, are highlighted. The primary proton transfer (1) is from the Schiff base to Asp85. A proton is released to the extracellular medium (2) by the proton release group, thought to be formed by Glu194, Glu204 and water molecules. The Schiff base is subsequently reprotonated from Asp96 (3) which is then reprotonated from the cytoplasmic medium (4). The final proton transfer step (5) from Asp85 to the proton release group (via Arg82) restores the ground state.

through isomerization of the retinal (Fig. 2A), and the resulting steric clash within the retinal binding pocket drives the subsequent structural rearrangements of the protein. These rearrangements correlate with a sequence of spectral changes which characterize the photocycle of bR (Fig. 2B). The red-shifted K-intermediate builds up within a few picoseconds at room temperature, followed by formation of the blue-shifted L-intermediate on a time scale of micro-

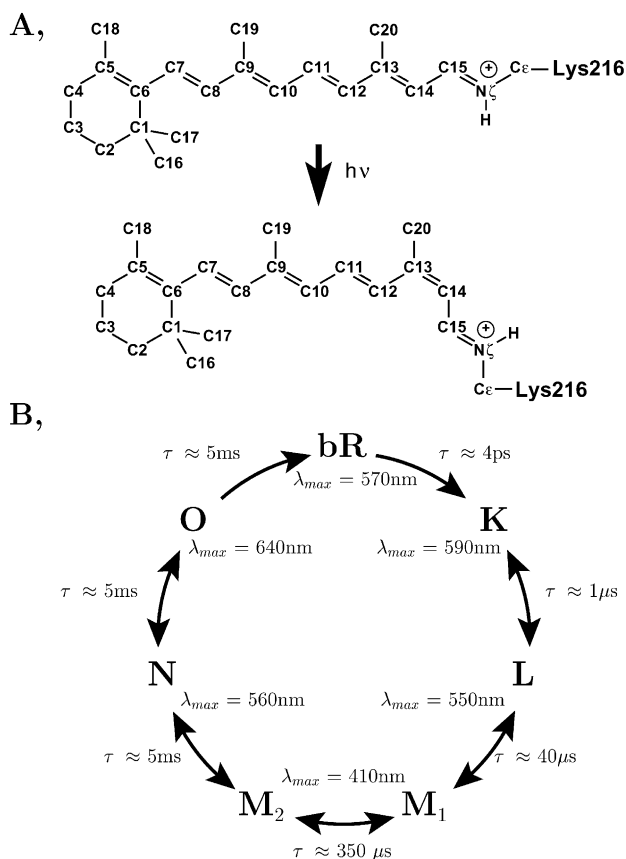


Fig. 2. Schematic representation of light-induced retinal isomerization and the bR photocycle. (A) The retinal chromophore is covalently bound to Lys216 via a protonated Schiff base. Following absorption of a photon the all-*trans* retinal is isomerized to the 13-*cis* configuration. (B) Retinal isomerization is the first event in the photocycle. The spectral intermediates, their absorption maxima, and their lifetimes at room temperature are shown.

seconds. The primary proton transfer event from the Schiff base to Asp85 (step 1 in Fig. 1) defines the L-to-M spectral transition, which induces a large blue shift in the absorption maximum. In wild-type bR under physiological conditions, a proton is released to the extracellular medium (step 2 in Fig. 1) on a similar time scale [20]. The identity of the proton release group is somewhat ambiguous, but is believed to be formed by Glu194, Glu204 and structural waters [21,22]. It is accepted that, on the sub-millisecond time scale, there is a spectrally silent transition [23] from an early M (labeled M₁) to a late M (labeled M₂), which is associated with a large structural rearrangement on the cytoplasmic side of the protein [24]. These changes ensure a switch in accessibility of the retinal, so that the Schiff base can subsequently be reprotonated from Asp96 (step 3 in Fig. 1) on the cytoplasmic side [25], corresponding spectrally to the M₂ to N transition. Asp96, in turn, is reprotonated from the cytoplasmic medium (step 4 in Fig. 1), and the absorption peak is further red-shifted as the retinal thermally re-isomerizes to recover the all-*trans* configuration, associated with the N to O transition. Finally, the ground state is recovered when a proton is transferred from Asp85 to the

putative release group on the extracellular side via Arg82 (step 5 in Fig. 1).

In this review, we discuss the new insights into the molecular mechanism of light-induced proton pumping which have emerged from several recent high-resolution structures. These were obtained by developing intermediate trapping protocols, and applying them to crystals of wild-type bR [26–29] and of bR mutants [30–32], as well as analysis of ground state structures of mutants of bR that may serve as structural analogues for the late intermediates in the photocycle [33,34]. While the basic picture outlined above is preserved, several important new details are revealed which shed light on the key steps of vectorial proton transport. In Section 2, we briefly sketch the most important results from the highest resolution structures of the ground state of bR which laid the framework for the intermediate trapping studies in 3-D crystals. In Section 3, we describe the different methodologies employed to structurally characterize in 3-D the intermediates of the bR photocycle. Section 4 presents the major structural results in progression, describing the early intermediate immediately following photoisomerization of the retinal chromophore; the sequence of events which set the stage for the primary proton transfer event from the protonated Schiff base to the primary acceptor Asp85; the coupled structural rearrangements which assist proton release to the extracellular medium; and the large-scale movements which facilitate the Schiff base reprotonation from Asp96 on the cytoplasmic side of the protein, as well as proton uptake from the cytoplasmic medium. Evidently, no single experiment yields the full story in its own right. Nevertheless, by combining the observed structural rearrangements and drawing comparisons with the wealth of biochemical, genetic and spectroscopic evidence, a coherent structural mechanism for light-induced proton pumping by bR emerges. Section 5 reviews an ongoing debate concerning the specific nature of the primary proton transport event. In closing, we summarize the overall structural mechanism and speculate to the extent that the central themes may be extended to aid the understanding of other ion translocation processes.

2. Structure of the ground state of bacteriorhodopsin

Discovered in 1967 [9] and having its functional role identified shortly afterward [10], the first electron crystallography structural model for bR [35], recovered from tilted 2-D samples, appeared as early as 1975. This remarkable pace of discovery, which resulted in bR being the first integral membrane protein from which any structural information was gleaned, was due to bR's natural propensity to form well-ordered two-dimensional crystals within the bacterial membrane of *Halobacterium salinarum*, combined with the development of electron crystallography as an important tool in structural biology. Nevertheless, it took a further 15 years before a high-resolution 3-D structure for

bR was published by Henderson et al. [15], and this stands out as a seminal contribution towards understanding the structural mechanism of bR. From this basis, a series of improved and refined electron crystallography structures followed [36–38], eventually achieving a resolution below 3 Å.

Three-dimensional crystallization experiments on bR were extensively performed, and appeared quite promising early on using detergent-solubilized bR [39]. Nevertheless, crystals were disordered and it was not until 1996 that the inception of a novel concept for the crystallization of membrane proteins utilizing the properties of lipidic cubic phases [40] resulted in the first well diffracting 3-D crystals of bR [41]. The reasoning underlying this approach was that membrane proteins might crystallize more readily in a lipid bilayer environment, provided that they could be incorporated into an appropriate matrix, retain their native properties, and diffuse in three dimensions. Bicontinuous cubic phases are highly viscous and transparent materials composed of lipids and water, and provide a stable, structured matrix in which diffusion of both water-soluble and membrane proteins takes place. It was suggested that labile membrane proteins, incorporated into continuous lipid bilayers, could be stabilized, diffusing rather freely along the bilayer, similar to the lateral diffusion of lipids. Upon nucleation, this “feeding” mechanism would eventually lead to well-ordered crystals. More details as to this crystallization technique and its general applicability may be found in recent references [42–46]. Other well-diffracting 3-D crystals of bR have since been grown from detergent-solubilized bR by epitaxy [16] and vesicle fusion [47].

The rapid pace of elucidation of the structural mechanism of bR which followed the development of lipidic cubic phase crystallization was unanticipated. In the intervening 5 years, X-ray structures of bR from lipidic cubic phase-grown crystals have been reported at 1.9 Å resolution [17] and 1.55 Å resolution [18]. Since the 1.9 Å structure was free from merohedral twinning, both structures are of similar quality and that at lower resolution is slightly more complete. These results were followed by the X-ray structures of the low-temperature K [26] (2.1 Å), L [27] (2.1 Å), and M (2.25 [28] and 2.0 Å [29]) intermediates of wild-type bR. In addition, M-state structures have been published for the D96N (2.0 Å) [30] and E204Q [31] (1.8 Å) bR mutants, as well as the ground state structure of the D85S bR mutant, claimed to model the O state (2.2 Å) [34]. All these studies used lipidic cubic phase grown crystals. Furthermore, high-resolution X-ray structures of hR [8] (1.8 Å) and SRII from *Natronobacterium pharaonis* (2.1 Å [48] and 2.4 Å [49]) have recently been described using the same crystallization approach. As such, the concept and implementation of lipidic cubic phase membrane protein crystallization [40] represents a significant contribution to understanding the structural mechanisms of the archaeal rhodopsin family. Since diffraction quality crystals of two bacterial reaction centers have also been reported using this technique [44], it

is not unreasonable to expect that X-ray structures of other membrane proteins may eventually be obtained using the lipidic cubic phase crystallization methodology.

Several important features have emerged from the X-ray structures of the ground state of bR at better than 2 Å resolution [17,18]. Most strikingly, the detailed atomic nature of the Schiff base’s complex counter ion, which stabilizes the high pK_a of 13.5 [50] of the Schiff base and the low pK_a of 2.2 [51] of the Asp85 was revealed, and is illustrated in Fig. 3. This counter ion is stabilized by a network of water-mediated hydrogen bonds which extends from the Schiff base, the primary proton donor, to the extracellular surface. A key water molecule, Wat402, forms H-bonds to the Schiff base nitrogen and the two negatively

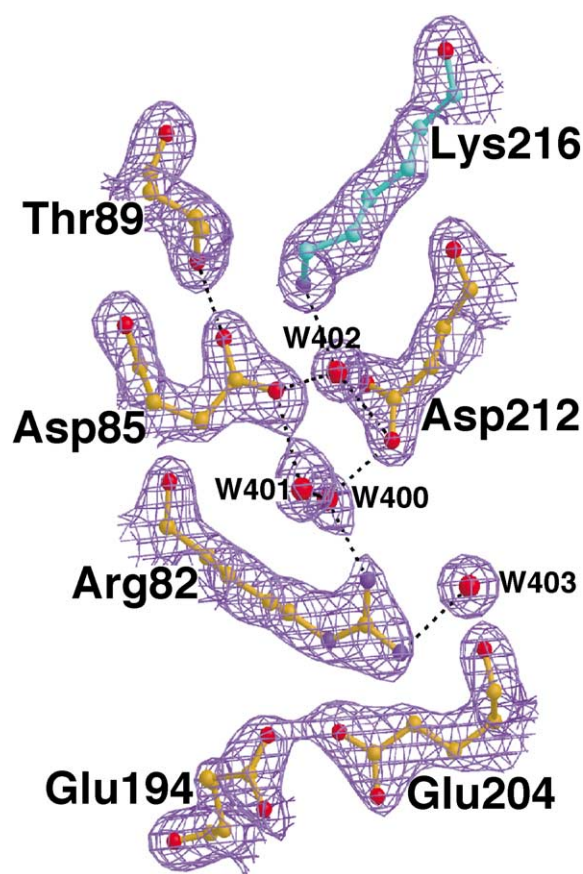


Fig. 3. Refined structure and electron density of the extracellular half of bR in the ground state. The $2F_{\text{obs}} - F_{\text{calc}}$ refined electron density map (blue, contoured at 1.2σ) shows the structure of the Schiff base’s complex counter ion formed by Asp85, Asp212, Wat400, Wat401, Wat402 and Arg82. The high pK_a of the Schiff base (13.5) is stabilized by a H-bond to Wat402 within the framework of this complex counter ion. The low pK_a of Asp85 (2.2) is stabilized by H-bonds to Thr89, Wat401 and Wat402. The close proximity of the positively charged guanidinium group of Arg82 also helps to stabilize the protonation states of both the Schiff base and Asp85. The proton release group is thought to be formed by Glu194, Glu204 and water molecules. The ground state model and crystallographic observations are available from entries 1qjh and 1lqjhsf of the protein data bank. Details are found in Ref. [17]. This figure was drawn using a modified version of Bobscript [130] and rendered using Raster3D [131].

charged aspartates (Asp85, the primary proton acceptor, and Asp212). As was anticipated by Gat and Sheves [52] through studies on model retinal compounds, within the framework of this complex counter ion, this water molecule stabilizes the unusually high pK_a of the Schiff base. Two further water molecules (Wat400 and Wat401) combine to form a pentagon, and link the two negatively charged aspartates to the positively charged guanidinium group of Arg82, which is located further away towards the extracellular surface, but in the ground state structure is orientated towards the active site. The presence of three H-bonds to Asp85 (O δ 2 receives a H-bond from Thr89 and O δ 1 receives H-bonds from Wat401 and Wat402) as well as the position of the positive charge of Arg82 stabilize the negative charge on the carboxylate group to the extent that the pK_a of Asp85 is 2.2 [51]. Arg82 in turn is connected through a series of H-bonds (Fig. 3) to the putative proton release group, formed by Glu194, Glu204 and water molecules [21,22].

Due to the 11 pK_a units difference between the primary proton donor and acceptor, even though these two groups share H-bonds to the same water molecule in the resting state, it is 10^{11} times more probable that a proton resides on the Schiff base rather than Asp85 under physiological conditions. These somewhat extreme pK_a values illustrate how the active site of bR has been optimized to ensure that Asp85 is not protonated by the nearby Schiff base, or by the extracellular medium prior to photoactivation. Similar arguments show that the Schiff base cannot be deprotonated by Asp85, any other nearby group, or by the cytoplasmic medium, guaranteeing the optimal protonation state in the bR resting state. It should be emphasized that this network of water-mediated H-bonds on the extracellular half of the protein (Fig. 3) also plays a significant structural role, making the extracellular half of the protein more rigid and brittle than the cytoplasmic half. An asymmetry in the distribution of flexibility has been observed in neutron diffraction studies [53] and is also reflected in the distribution of crystallographic temperature factors [16–18], which are systematically lower on the extracellular half of the protein.

Whereas several well-defined water molecules appear along the proton translocation channel on the extracellular side of the protein (Fig. 3), on the cytoplasmic side there are relatively few. One conserved water (Wat501) appears between Trp182 and Ala215 [17,18], and another crystallographic water (Wat502) was identified near the carbonyl oxygen of Lys216 [18]. An H-bond from Ala215 to Wat501 creates a local distortion of the H-bond pattern of helix G in this region, and this was recently assigned as a π -bulge [18], providing a more detailed description of the bend in helix G which was seen as early as 1990 in the electron crystallography structure [15]. With the exception of Asp96 and Thr46, which share a H-bond, the cytoplasmic half of the proton translocation channel consists predominantly of hydrophobic residues. These pack tightly against each other and create a hydrophobic barrier preventing the leakage of

protons back across the membrane, which would otherwise dissipate the energy stored within the proton-motive potential. Nevertheless, it is necessary that a proton enters the proton translocation channel from the cytoplasm during the latter half of the photocycle. To assist this, the four aspartates at the cytoplasmic surface of bR (Asp36, Asp38, Asp102 and Asp104) serve to attract protons from the cytoplasm. In addition, a number of 2-D studies of photoactivated bR in projection [24,54–61] have firmly established that a large-scale movement of helices on the cytoplasmic half of the protein occurs following the deprotonation of the Schiff base, which opens up this hydrophobic barrier to the cytoplasmic medium.

Several other details regarding the interactions between the bR molecules within the trimer, or interactions with lipid molecules [16–18], have also emerged from the higher resolution structure and are reviewed elsewhere [45,62].

3. Intermediate trapping and mutation protocols

Structural characterization of any reaction intermediate within crystals requires that the protein is functionally active in the crystalline state and that conditions can be found under which a sufficient population of the desired intermediate builds up [63]. In the case of lipidic cubic phase grown 3-D crystals of bR, the protein packs in purple membrane-like layers that are stacked along the direction perpendicular to the plane of the membrane. Fourier transform infrared (FTIR) studies have established that bR's photocycle in 3-D crystals closely resembles that of bR in the native purple membrane [64]. A common strategy for trapping structural intermediates of light-driven macromolecules has been to illuminate 3-D crystals at low temperature [65–68], although reaction initiation at room temperature [69], as well as pump-probe experiments using a broad spectrum X-ray probe [70,71], have also been reported. Other strategies are to select a mutant for which the decay of the desired intermediate is slowed, and thereby recover a relatively high population of this intermediate. Alternatively, one may determine the structure of a mutant (or mutants) for which there are reasons to believe that its ground state structure models a specific photo-intermediate. In the last 3 years, structural results for the intermediates of the bR photocycle have been reported using all of these approaches, with the exception of room temperature pump-probe studies which appear unlikely to succeed due to rapid disordering of the crystal lattice.

Studies of the dynamics of bR at low temperature have established two phase transitions that occur as a function of temperature, corresponding to distinct changes in the nature of the allowed motions. As shown in Fig. 4, the first phase transition is at 150 K, where a change in the linear dependence of the mean square amplitude of motion with temperature sets in [53], and was observed by Zaccai et al. using neutron scattering. A second phase transition occurs at 240

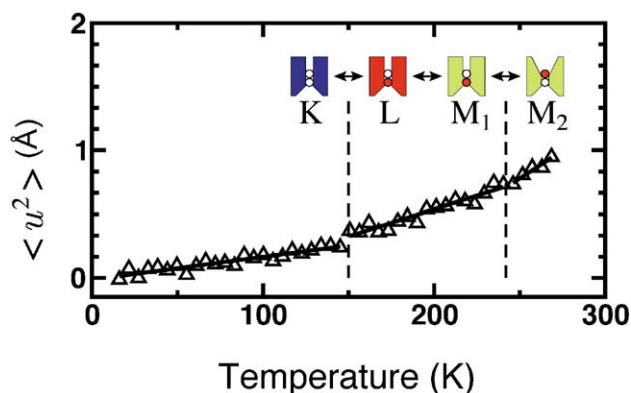


Fig. 4. Low-temperature dynamics of bR. Hydrogen mean square amplitudes (y -axis) measured by neutron scattering are plotted as a function of temperature (x -axis). Experimental and theoretical details are given in Ref. [53]. A phase transition is visible at 150 K and (possibly) at 240 K, representing a change in the nature of the allowed motions. The phase transition at 240 K switches the accessibility of the Schiff base from the extracellular to the cytoplasmic side [72]. A correlation with low-temperature studies of the bR photocycle intermediates is represented schematically. Illumination of bR at 110 K is commonly used to generate and trap the K-intermediate; likewise, illumination of bR at 170 K is commonly used to trap the L-intermediate; at 230 K to trap the early M-intermediate; and illumination above 240 K is used to trap the late M, as well as the later intermediates. The K, L, M₁ and M₂ photo-intermediates and their accessibility are shown schematically. For K, L and M₁, the cytoplasmic (upper) half of the proton translocation channel is closed, but becomes open in M₂. Photoisomerization breaks the accessibility to the extracellular side below 150 (denoted schematically as two white circles), but the Schiff base becomes accessible to the extracellular side (lower circle red) above 150 K, and switches its accessibility to the cytoplasmic side (upper circle red) above 240 K [72]. Experimental data from Ref. [53] is reproduced with permission from G. Zaccai. The schematic representation of the intermediates and their accessibility are modified from those of Ref. [24].

K, and was first identified using FTIR spectroscopy [72]. In that work, Ormos established that the retinal, when deprotonated, becomes reprotonated from the extracellular side of the protein below 240 K, but from the cytoplasmic side above 240 K. Evidence for a phase transition at 240 K is also suggested in the neutron scattering data [53] (Fig. 4). As is illustrated schematically in Fig. 4, there exists a correlation between the temperature at which these phase transitions occur, and the temperature at which specific photo-intermediates become populated when bR is illuminated.

A generally accepted protocol for trapping the K-intermediate at low temperature (K_{LT}) is to illuminate bR with green light near (or below) 110 K [73–75]. Similarly, most low temperature studies on the L-intermediate have either illuminated bR with red light at 170 K [76–82], or have first illuminated bR with green light at lower temperature and then warmed the sample up to 170 K [83]. It is necessary to raise the temperature to at least 150 K in order to ensure that the protein has sufficient thermal energy to cross the energy barrier associated with the K to L transition, and this correlates with a distinct change in the nature of the allowed motions above 150 K [53] (Fig. 4). Similarly, 2-D structural

studies in projection on the M-intermediates of bR have shown that while no large-scale structural rearrangements have been reproducibly observed below 240 K [75,81], studies performed at 240 K or above have repeatedly observed significant movements near the cytoplasmic sides of helices E, F and G [24,54–61]. These movements, which are characteristic of the spectrally silent M₁ to M₂ transition (Fig. 2B), correlate with the phase transition observed at 240 K, in which the accessibility of the Schiff base switches from the extracellular to the cytoplasmic side [72]. As such, any protocol for trapping the M₂ (or a later) intermediate of the bR photocycle must ensure that the temperature is raised

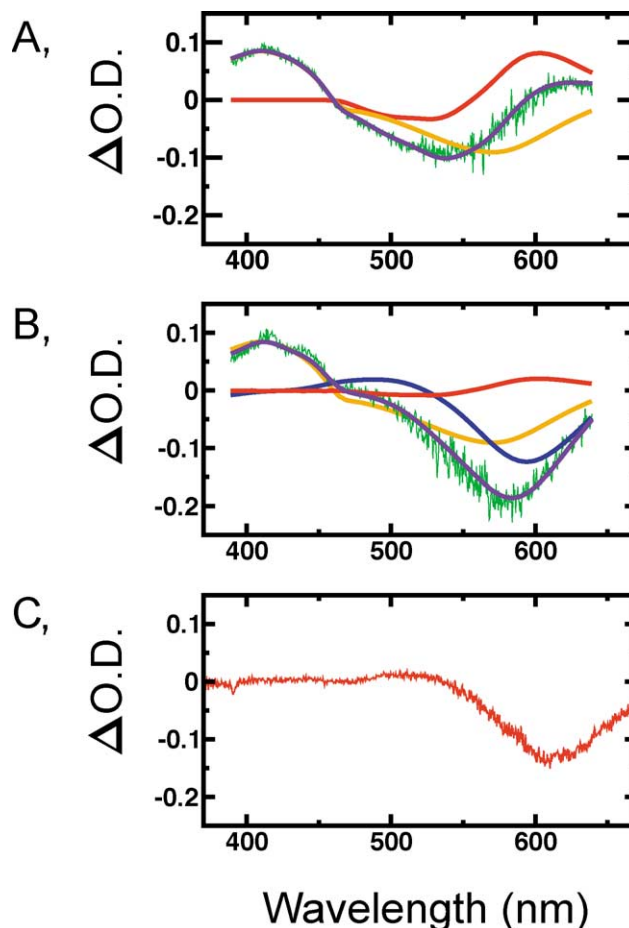


Fig. 5. Difference spectra recorded from single 3-D bR crystals at low temperature. (A) Following 30 s illumination with green ($\lambda = 532$ nm) light at 170 K, the difference spectrum (green) shows a mixture of K_{170K} (red) and M_{170K} (orange) in the ratio of 4:1. (B) After a further delay of 40 s in the dark, this evolved to the difference spectrum (green) yielding a mixture of 1:3:1 for the K_{170K} (red): L_{170K} (blue): M_{170K} (orange) spectral intermediates, with L_{170K} becoming the dominant species. The purple lines give the spectral decomposition. (C) Following 30 s illumination with red ($\lambda = 635$ nm) light at 150 K plus a further delay of 40 s in the dark, the difference spectrum (red) is characteristic of an almost pure L_{150K} . The changes in electron density which resulted when following the trapping protocols B and C are shown in Fig. 6C and B, respectively. Details of the spectral decomposition are given in Ref. [85]. Data shown in A and B are reproduced with permission from Photochemistry and Photobiology.

above 240 K for a sufficiently long period such that large-scale rearrangements can occur.

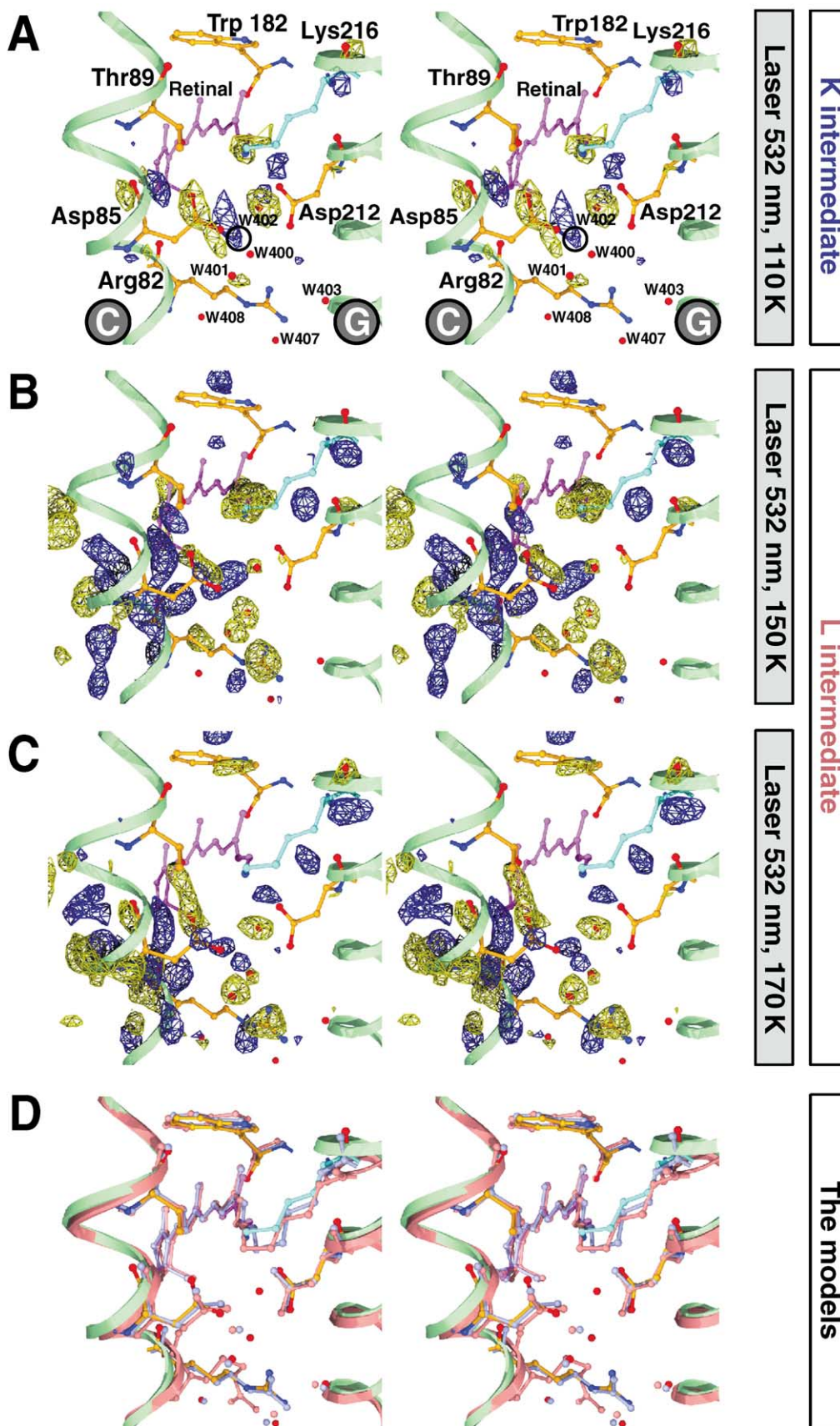
In our work on the low-temperature K-intermediate of bR [26], we used green light to illuminate 3-D crystals cooled to 110 K in a stream of nitrogen gas. Green light illumination established a photostationary state containing a substantial population of $K_{110\text{ K}}$ [73,74], which was characterized spectrally using single crystal microspectrophotometry [84]. The long-distance view of the difference Fourier map [26] showed the structural rearrangements to be clustered in the immediate vicinity of the active site, as was also the case in studies on an early intermediate of photoactive yellow protein [67]. Crystallographic refinement with partial occupancy established that 35% $K_{110\text{ K}}$ was trapped in 3-D crystals under these conditions.

In characterizing the structural changes associated with the low-temperature L-intermediate [27] we worked at 170 K [76–82]. We used green light illumination for 30 s followed by a further 40 s delay in the dark, at which point we froze crystals in liquid nitrogen and later mounted them in the X-ray beam. Fig. 5A shows the difference spectrum of the photostationary state after 30 s illumination with green light, which indicates a mixture of 48% $K_{170\text{ K}}$ and 12% $M_{170\text{ K}}$ [85]. After a further 40 s delay in the dark, during which most of the $K_{170\text{ K}}$ evolved to $L_{170\text{ K}}$ (Fig. 5B), the crystals exhibit a mixture of 12% $K_{170\text{ K}}$, 36% $L_{170\text{ K}}$ and 12% $M_{170\text{ K}}$ [85]. The long-distance view of the difference Fourier map [27] showed that the structural rearrangements evolved along the proton translocation channel towards the extracellular medium. Since the illumination conditions were similar to those used for trapping $K_{110\text{ K}}$, the structural evolution we observed from $K_{110\text{ K}}$ to $L_{170\text{ K}}$ (Fig. 6) arose from the extra thermal energy at 170 K, which correlates with the phase transition at 150 K [53] (Fig. 4). Crystallographic refinement with partial occupancy converged from above and from below to a value of 70% for the trapped photo-intermediate species [27,85], and the well-ordered structure (Fig. 8 shows the $2F_{\text{obs}} - F_{\text{calc}}$ electron density map) was labeled L_{LT} in recognition of the fact that this

was the predominant intermediate trapped, although the presence of a small component of M_{LT} was acknowledged in the publication [27]. An apparent discrepancy between the population estimates deriving from the spectroscopic (60%) and crystallographic (70%) analyses stems from the limitations of both techniques [85], since the white light probe used to record a difference spectrum unavoidably shoots a fraction of the trapped species back to the ground state, whereas partial occupancy refinement with the ground state model held fixed tends to overestimate slightly the population of the intermediate species.

Since the publication of this structural result [27], it has been suggested that the total trapped population, based on spectroscopy alone, was approximately 30%, and hence the X-ray crystallographic result contained a dominant (rather than a minor) contribution from the M-intermediate [86–88]. These spectral assignments, which account for less than 50% of the total population of the trapped intermediate [27,85], were based upon the assumption that spectra recorded from 3-D crystals of bR at 170 K are identical in all respects to those recorded from purple membrane samples in suspension at other temperatures and pH. It is well known that absorption spectroscopy of proteins can depend on the medium in which they reside, the pH and the temperature. Specifically, spectra recorded from 3-D crystals often differ from those recorded from samples in suspension [89–91] and this is also true for 3-D crystals of bR grown in a lipidic cubic phase. In keeping with this, the maximum extinction of the M-intermediate at 410 nm in 3-D crystals of the D96N bR mutant [62] was equal to that of the ground state peak at 570 nm, although scatter at short wavelengths somewhat affected the spectral observations. That the spectral fingerprint for the M-intermediate at 410 nm in 3-D crystals of wild-type bR cooled to 170 K [85] is strong relative to its fingerprint in samples in suspension at higher temperatures was central to this issue, and has been elaborated upon through a more detailed spectral analysis [85]. Furthermore, illumination of 3-D crystals of bR with red light at 150 K results in a significant population of $L_{150\text{ K}}$,

Fig. 6. Evolution of structural changes resulting from photoactivation of bR at low temperature, overlaid (in A, B and C) on the ground state bR model. Positive and negative difference electron densities are shown in blue and yellow, respectively. (A) Stereo view of the difference Fourier map resulting from illumination of a single 3-D crystal of wild-type bR with green ($\lambda = 532\text{ nm}$) light at 110 K contoured at 4σ ($\sigma = \text{r.m.s. electron density for the unit cell}$). These changes characterize the K_{LT} intermediate. A negative difference electron density peak indicates the disordering of Wat402, as is a weaker peak visible on Wat401. Paired negative and positive difference electron density peaks indicate a small movement of Asp85 towards the Schiff base as well as movements of the side chain and backbone of Lys216. The circle between Asp85, Wat400 and Wat402 highlights positive difference electron density which may correlate with the reordering of one disordered water molecule. (B) Stereo view of the difference Fourier map resulting from 30 s illumination of a 3-D bR crystal with red light at 150 K, followed by a delay of 40 s prior to quenching in liquid nitrogen. This map is contoured at 2.8σ . (C) Stereo view of the difference Fourier map resulting from 30 s illumination of a 3-D bR crystal with green light at 170 K, followed by a delay of 40 s prior to quenching in liquid nitrogen. This map is contoured at 3.4σ . B and C show similar structural rearrangements, which characterize the L_{LT} -intermediate. Negative electron density peaks arise on Wat400, Wat401 and Wat402, and (in C) a positive peak is visible at the center of this triad. Both maps show paired negative and positive difference density peaks corresponding to a reorientation of the guanidinium group of Arg82 towards the extracellular medium. Extended paired negative and positive electron density peaks stretch along the backbone of helix C, indicating a local flex of this helix towards the proton translocation channel. Electron density peaks indicating a movement of the side chain of Trp182 towards the cytoplasm are also visible. (D) Structural models for K_{LT} (blue, a refinement with fewer constraints, crystallographic observations are available from entries 1QKO and 1QKP of the protein data bank) and L_{LT} (red, model and crystallographic observations are available from entry 1EPO of the protein data bank) overlaid on the ground state (green backbone and colored residues, model and crystallographic observations are available from entries 1qhj and 1qhjsf of the protein data bank). All the major changes described above are reproduced through crystallographic refinement. This figure was drawn using the Swiss PDB Viewer [132].



whereas those of $K_{150\text{K}}$ and $M_{150\text{K}}$ are negligible (Fig. 5C). It was therefore decisive that the analysis of the X-ray diffraction data to 2.3 Å recorded following this trapping protocol (Fig. 6B and C show the difference Fourier maps recovered using the red and green light trapping protocols, respectively) reproduced the earlier structural result [27].

Four studies have recently reported X-ray structures of the M-intermediate from wild-type bR [28,29], and from the D96N [30] and E204Q [31] bR mutants, all using 3-D crystals grown in a lipidic cubic phase. The trapping protocols for three of these studies [28,30,31] were similar, but they differed markedly from protocols successfully used to observe large-scale light-induced movements in bR [24,54–61]. bR crystals were first frozen in liquid nitrogen and then mounted in a cryo-cooled stream of nitrogen gas. The cold nitrogen stream was subsequently blocked for a short period of time, during which crystals thawed and were simultaneously illuminated with either yellow [30,31] or green [28] light. After either 1 [28,31] or 3 s [30] the object used to block the nitrogen gas stream was removed and crystals were refrozen. No characterization of the thermal history of crystals when following this protocol has been presented. The observation in the case of the E204Q mutant that X-ray diffraction data could be integrated with identical unit cell parameters to those of the ground state [31] suggests that either the final temperature reached, or the time interval at this temperature, was not sufficient to allow large-scale structural rearrangements of the protein during the second in which the crystal thawed. Curiously, this protocol yielded a structure of the early M_1 intermediate for the E204Q mutant rather than the O-intermediate which is expected when working with this bR mutant at room temperature [21]. A very similar trapping protocol for wild-type bR yielded a mixture of 35% bR, 30% M_1 and 35% M_2 [28]. More consistent with studies on bR mutants at room temperature, a period of 3 s for thawing and illuminating 3-D crystals of the D96N bR mutant produced almost 100% M_2 [30]. Unfortunately, in this case, the electron density was so disordered that the cytoplasmic portions of helices F and G, which show the largest movements and are therefore of the greatest mechanistic significance, were excluded from the model. A distinctly different trapping protocol was used by Facciotti et al. [29] who first illuminated wild-type bR crystals for 3 min at 230 K, and then quenched them in liquid nitrogen prior to X-ray diffraction data collection. Since this temperature lies below the phase transition at 240 K [72] (Fig. 4) an early M_1 intermediate would be expected. The structure which was recovered [29] was in good agreement with the early M of the E204Q mutant [31], illustrating (as in the case of red light illumination at 150 K versus green light at 170 K, Fig. 6) that the same structure for a specific intermediate can be recovered using different trapping protocols.

In recovering 3-D structural information from the N-intermediate, Vonck [32] illuminated 2-D samples of the F219L bR mutant for 30 s at 270 K prior to plunging the

sample into liquid nitrogen. This protocol recovered a population of 33% for the trapped N-intermediate, as would be expected for the photostationary state under the conditions used. At 270 K, large movements associated with the cytoplasmic sides of helices E, F and G were observed. These movements did not occur when 3-D bR crystals were illuminated at lower temperatures [26,27,29] and they correlate with the phase transition at 240 K [72], which serves to switch the accessibility of the Schiff base from the extracellular to the cytoplasmic side.

Another approach for glean structural information concerning the second half of the bR photocycle (Fig. 2B) has been to determine the ground state structure of bR mutants which serve as models for the later intermediates. Subramaniam and Henderson [33] recently reported the electron crystallographic structure of the D96G/F171C/F219L triple mutant of bR. Justification for this approach derives from 2-D electron diffraction studies in projection which demonstrated that, for this specific triple mutant, the full extent of the light-driven conformation change associated with the late M_2 intermediate of the bR photocycle is present even without illumination [24]. As such, and despite the shortcomings of using a triple mutant analogue rather than a trapped photocycle intermediate, this approach yielded the most reliable structure for the open conformation of bR to date. The same philosophy has been applied to argue that the X-ray structure of the ground state of the D85S bR mutant provides a model for the O-intermediate of bR [34]. In contrast to the work of Subramaniam and Henderson [24,33], this conjecture is not supported by structural studies of the D85S bR mutant and the O-intermediate of bR in projection. Rather, an appeal is made to the 2-D structure of the D85N bR mutant at high pH, which appears to exhibit an M-like conformation [92]. While the structure of the D85S bR mutant is of interest in its own right, as this mutation (like the D85T bR mutant) converts the protein to an inwardly directed chloride pump [93], its structural link to the O-intermediate of the bR photocycle does not appear to be well founded.

4. Structural evolution of bR: resolving a revolving photocycle

In an ideal case, high-resolution X-ray structures from wild-type bR crystals free of merohedral twinning and at 100% occupancy would be reported for every intermediate in the photocycle (Fig. 2B). Despite the fact that all experiments described above fall short of this ultimate case, when viewed with an acceptance of the limitations of the technique, the structural results themselves present a remarkably consistent picture of the structural evolution during the first half of the bR photocycle [26,27,29,31]. Unfortunately, the X-ray crystallographic results from the later intermediates have been in conflict both with each other [28,30,34] and

with those derived from electron diffraction studies [32,33]. Nevertheless, although at lower resolution, a reliable 3-D model for the conformation of bR which is open to the cytoplasm is provided by the electron crystallography structure of the D96G/F171C/F219L triple mutant of bR [33], and the major conclusions drawn from this work are well-supported by the 3-D model of the N-intermediate of the F219L mutant [32]. From these results, in combination with a wealth of spectral, genetic and biochemical data, a molecular level 3-D movie of bR in action [94] can be pieced together and is described below.

4.1. Low-temperature X-ray structure of K

At room temperature, the K-intermediate builds up within a few picoseconds following photoisomerization of the retinal (Fig. 2). Of particular interest is that the C₁₃=C₁₄ bond of the retinal chromophore is isomerized [95,96] and therefore the energy requirements for proton transport uphill against a proton-motive potential must already be apparent as either structural rearrangements or strain on the retinal. When observing limited structural changes, Henderson and Moffat [97] have shown that difference Fourier methods provide the most sensitive and least biased method of analysis. For this reason, it has become almost universal to present a difference Fourier map when describing structural changes in light-driven macromolecular systems [26–28,65–68,70,71]. One significant advantage of the method is that, when a long-distance overview of the map is presented [26,27,67], the background noise level of the map can be seen by inspection, since regions of the protein removed from the active site provide an internal control. Overviews of the difference Fourier maps for K_{LT} and L_{LT} can be found in our references [26,27] but were not presented by other workers in the field in their work that is described below.

Fig. 6A shows the difference Fourier map for K_{LT} near the active site, and Fig. 6D shows the refined K_{LT} model (blue). Paired positive and negative electron density peaks near the side chain and carbonyl oxygen of Lys216 illustrate how its side chain and main chain move in response to retinal isomerization. A movement of the side chain atoms may have been anticipated from the fact that N_ζ of Lys216 (i.e. the Schiff base nitrogen) is covalently bound to C₁₅ of the retinal (Fig. 2A) and necessarily undergoes a significant movement in response to photoisomerization about the C₁₃=C₁₄ bond. That a physical pull of the retinal through the side chain of Lys216 also results in a movement of the backbone may in part be facilitated by a weakening of the H-bond formed by this carbonyl oxygen due to a local π-bulge of helix G in this region [18]. In addition, the polyene chain and β-ionone ring of the retinal are firmly held in place by bulky hydrophobic residues which form a closely packed binding pocket, hence the retinal itself cannot undergo large movements so as to relieve strain [98,99]. An early indication of strain within the retinal which would

serve to store energy in K_{LT} and later be released as the photocycle evolved is the observation that retinal isomerization induces a steric clash of its C₁₃ methyl group with Trp182 on helix F [26]. At 2.1 Å and 35% occupancy, however, the extent to which the retinal was twisted could not be observed and planar constraints were applied during refinement. Resonance Raman spectroscopy has established that the retinal is strained in K, somewhat more so at low temperature than at room temperature [96].

The strongest negative electron density peak in the difference Fourier map arose on Wat402 (Fig. 6A), indicating that this key water molecule, which in the ground state [17,18] was hydrogen bonded to the Schiff base, Asp85 and Asp212 (Fig. 3), becomes disordered in response to retinal isomerization. This result is consistent with FTIR studies at low temperature which also demonstrate that the Schiff base H-bond is lost in K_{LT} [99]. There are two factors which combine to dislodge this water molecule. In the first instance, retinal isomerization reverses the orientation of the N–H dipole of the Schiff base, which served as a H-bond donor to Wat402 in the ground state model, but cannot do so when the retinal is isomerized. In the second instance, retinal isomerization induces a movement of the side chain of Lys216 (Fig. 6A) such that it swings across and “kicks out” this water molecule (Fig. 7) like a football player striking a football. In the refined model (Fig. 6D), the

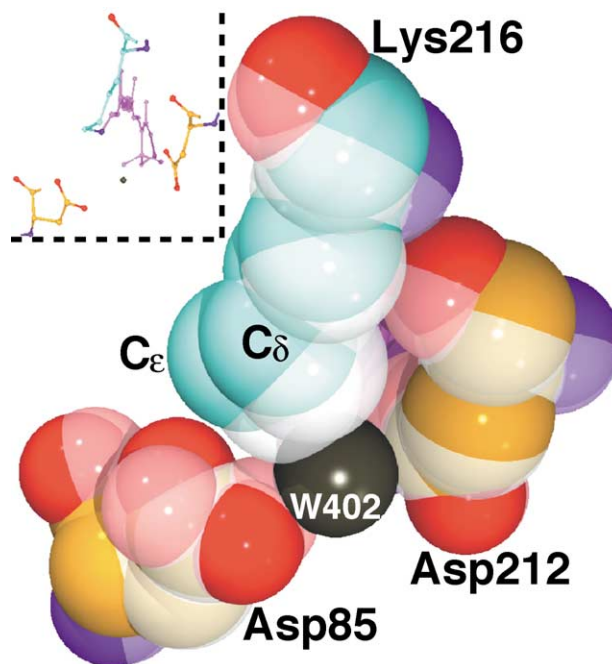


Fig. 7. Structural mechanism for the disordering of Wat402 in the active site in the K_{LT} intermediate. A space filling representation of the ground state (colored) and K_{LT} (white) models show that, due to the photoisomerization of the retinal, the movement of C_ε of Lys216 induces a steric clash with Wat402 (black). Consequently, this water molecule is displaced. The upper left part shows the active site orientation in a ball and stick representation. This figure was drawn using the Swiss PDB Viewer [132].

distance from C_ϵ of Lys216 to the position originally occupied by Wat402 is 2.3 Å, which results in a steric conflict (highlighted in the space filled model, Fig. 7) since this C_ϵ cannot serve as a H-bond donor to Wat402. In the difference Fourier map for K_{LT} , there is positive density in a position between Asp85 and Asp212 (Fig. 6A), overlapping with a positive feature found in the L_{LT} map (Fig. 6C), which may correspond to reordering of this water molecule. This rearranged water molecule (Fig. 6D, blue) is also seen for all later intermediates [27–31]. A weaker negative difference electron density peak appears on Wat401 in K_{LT} (Fig. 6A), indicating that a movement of Wat402 is also communicated to this water molecule. An early movement of Asp85 towards the position originally occupied by the Schiff base is also apparent as paired negative and positive difference electron density peaks near this residue. These slight movements were not resolved in the difference Fourier electron diffraction map resulting from green light illumination of bR at 77 K [75].

One appealing consequence of the postulate that a steric clash of C_ϵ of Lys216 contributes to dislodging Wat402 is that it also suggests why isomerization about the $C_{13}=C_{14}$ double bond (Fig. 2A) initiates a sequence of events resulting in the translocation of a proton across the cell membrane, whereas isomerization about the $C_{15}=N_\zeta$ double bond (which corresponds to dark adaptation of bR [100]) does not. A simple model for the dark-adapted state does not reveal this steric clash of C_ϵ with Wat402 and therefore it is likely that this water remains well-ordered in the dark-adapted state. All high-resolution X-ray structures of the later intermediates [27–31] are consistent with these observations for K_{LT} since all show movements of Wat402, Asp85 and Lys216. From an energetics viewpoint, it is appealing that two energetically expensive tasks are fulfilled early in the photocycle, namely the disruption of three H-bonds to Wat402 and the weakening of a H-bond formed by the carbonyl oxygen of Lys216. By achieving these tasks before the energy absorbed by the photon is thermally dissipated, the stage is set for more extensive structural rearrangements later in the photocycle.

4.2. Low-temperature X-ray structure of L

At room temperature, the L intermediate builds up in the microsecond time range (Fig. 2B) and governs the primary proton transfer event from the Schiff base to Asp85 (Fig. 1). A strong case can be argued that the structure of the L intermediate is decisive when seeking to understand the mechanism of vectorial transport by bR. Most strikingly, only the removal of the retinal or the mutation of Asp85 to a neutral group are effective in preventing bR from pumping protons [101]. Changes in the temperature, pH, or the mutation of any other charged residue along the proton transport channel (Fig. 1) [20] affect the photocycle kinetics and can alter the order of specific events. Nevertheless, bR's ability to translocate protons is quite tolerant of these

perturbations. For these reasons, an increased emphasis has recently been placed upon the primary proton transfer event as central to vectoriality in the proton pumping mechanism [27,33,85,102,103].

A structural model for L must explain three remarkable features of this intermediate. In the first instance, whereas the K intermediate builds up in the picosecond time range (Fig. 2B), there is a delay of six orders of magnitude before K decays into the L intermediate. This difference makes the K intermediate by far the relatively longest lived intermediate in the bR photocycle. In the second instance, structural changes associated with the L intermediate must serve to reverse the proton donor/acceptor relationship of the Schiff base and Asp85. As described in Section 2, the ground state structure stabilizes the high pK_a (13.5) of the Schiff base [50], and the low pK_a (2.2) of Asp85 [51]. By L, the pK_a of the Schiff base must be reduced, and that of Asp85 increased, to the point where a proton can exchange between these oppositely charged groups in the L to M transition. Finally, retinal isomerization reverses the orientation of the Schiff base N–H dipole away from the extracellular side of the protein and towards the cytoplasmic side. The structure of L must imply a mechanism whereby a low barrier pathway for proton exchange can be defined, such that the Schiff base becomes transiently accessible to Asp85 on the extracellular side.

Fig. 6C shows the difference Fourier electron density map dominated by $L_{170\text{ K}}$ [27,85], and the refined structure is shown in Fig. 6D (red). As expected, the structural changes observed in $K_{110\text{ K}}$ (Fig. 6A) propagate out from the active site towards the extracellular medium in $L_{170\text{ K}}$ (Fig. 6C). As with $K_{110\text{ K}}$, paired positive and negative peaks arise near the carbonyl oxygen of Lys216, and a strong negative electron density peak is apparent for Wat402 in $L_{170\text{ K}}$. In addition, in $L_{170\text{ K}}$ considerably more structural rearrangements are apparent. Strong negative peaks are now also observed on Wat400 and Wat401, which have dislocated, as is a positive electron density peak visible, indicating the reordering of one water molecule [27] near the center of this triad of ground state water molecules. Furthermore, paired negative/positive electron density peaks clearly show that the positively charged guanidinium group of Arg82 has reoriented towards the extracellular medium. However, the most striking feature of the difference Fourier map is the presence of well-defined positive and negative electron density peaks along the backbone of helix C, extending from Ala81 to Phe88 (Fig. 6C). These features were interpreted as stemming from a local flex of helix C, which exaggerates a small movement of Asp85 towards the Schiff base already apparent in K_{LT} (Fig. 6A). The disruption of three H-bonds on the extracellular side of the protein after photoexcitation at 170 K [27] which were not disrupted at 110 K [26] is due to the increased thermal energy of the protein and surrounding solvent at this temperature, and this correlates structurally with the phase transition at 150 K [53] (Fig. 4).

As shown in Fig. 5C, when using red light illumination at 150 K rather than green light illumination at 170 K, there is a strong spectral contribution from $L_{150\text{ K}}$ but that from $K_{150\text{ K}}$ or $M_{150\text{ K}}$ is negligible. Fig. 6B shows the difference Fourier map which resulted from red light illumination of a 3-D crystal at 150 K. Although this map is noisier than that obtained following our green light illumination protocol [27] (Fig. 6C) due to the lower total occupancy of the trapped intermediates, it is fully consistent with the difference Fourier map previously reported. The choice between either trapping protocol demands a compromise, with that using red light favoring spectral purity at the expense of greater noise in the crystallographic electron density map, whereas that using green light minimizes the crystallographic noise at the expense of a greater mixture of states in the difference spectrum. While our original publication reflected our own bias within this context [27], crystallographic refinement establishes that both protocols yield the same structure for the low-temperature L-intermediate. These movements were not resolved in the difference Fourier electron diffraction map in projection resulting from red light illumination of bR at 170 K [81].

In Fig. 8 the $2F_{\text{obs}} - F_{\text{calc}}$ electron density map and refined model for $L_{170\text{ K}}$ are shown. Since the trapped intermediate had a crystallographic occupancy of 70% [27,85] all significant features of the difference Fourier map, such as rearrangements of water molecules, reorientation of Arg82, and the local flex of helix C, are immediately visible within the well-ordered electron density. There are compelling reasons to believe that the structures of $L_{170\text{ K}}$ and $M_{170\text{ K}}$ are very similar [29,72,85], not the least being the fact that a single structural intermediate provided an excellent model for the observed electron density (Fig. 8). It is curious to note that, whereas our trapping protocol produced a mixture of spectral intermediates yet well-ordered electron density (Fig. 8), the opposite occurred for the late M-state of the D96N bR mutant, for which a spectrally pure species was trapped [62] but the electron density was disordered to the point that vital regions were excluded from the model [30].

Our observation that a local rearrangement of a secondary structural element (i.e. a flex of helix C) is associated with the K-to-L transition explains why a time scale of microseconds (rather than nanoseconds) is required for this spectral transition (Fig. 2B). Furthermore, our X-ray model provides a global picture incorporating the suggestion that Asp85 approaches the Schiff base in L [79,102] which derived from solid-state NMR spectra recorded at 170 K. In addition, a structural basis for the 40 nm blue shift associated with the K-to-L transition is revealed. As established through studies of a number of retinal salts by Albeck et al. [104], the spectral shift depends critically on the distance between the protonated Schiff base and the primary counter ion (Asp85 in bR), with a blue shift resulting as the two approach one another. Furthermore, the reorientation of the guanidinium group of Arg82 away from the Schiff base

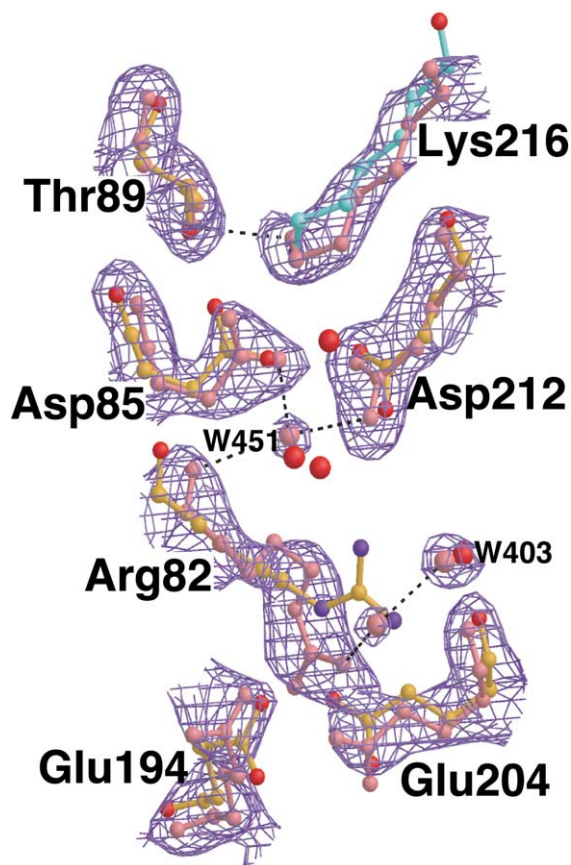


Fig. 8. Refined structure (red) and electron density (blue) of the extracellular half of L_{LT} overlaid on the ground state model (colored). The $2F_{\text{obs}} - F_{\text{calc}}$ refined electron density map (contoured at 1.0σ) reveals that the Schiff base's complex counter ion (Fig. 3) is considerably disrupted prior to proton transfer. The three H-bonds between Asp85 and Thr89, Wat401, and Wat402 are lost, and a new water molecule (Wat451) reorders between Asp85 and Asp212. The side chain of Arg82 reorients towards the extracellular medium, and the backbone carbonyl oxygen of Arg82 moves into a position where it can compete with Asp85 as a H-bond acceptor from Wat451. A local flex of helix C exaggerates the movement of Asp85 towards both the Schiff base and Asp212. These structural rearrangements increase the pK_a of Asp85 to the point where it becomes a proton acceptor relative to the photoisomerized Schiff base. Since the well-ordered electron density corresponds to the structure of L_{LT} (red) rather than the ground state model (colored) it is apparent that the occupancy of L_{LT} is significantly greater than 50%. The model for L_{LT} and the crystallographic observations are available from entry 1EPO of the protein data bank. Details are found in Refs. [27] and [85]. This figure was drawn using a modified version of Bobscript [130] and rendered using Raster3D [131].

also contributes to the spectral shift [48,49,105]. These factors combine to produce a significant blue shift, which may in part be compensated by a reduction of strain on the retinal [102]. Unfortunately, as with the structure of K_{LT} , at 2.1 Å resolution, it was not possible to observe the extent to which the retinal was twisted and (of necessity) constraints were imposed during refinement.

Considerable insight into how the proton donor/acceptor relationship of the Schiff base and Asp85 is reversed prior to proton transfer is gained from the structure of L_{LT} . As

described in Section 2, the high pK_a of the Schiff base is stabilized in the ground state by a H-bond to Wat402 (Fig. 3). That a H-bond from the Schiff base to a strategically placed water molecule could yield an unusually high pK_a (13.5) for this group was anticipated by Gat and Sheves [52] through studies on model retinal compounds. Upon formation of the K intermediate, retinal isomerization disorders this key water molecule [26] (Fig. 6A) and reorientates the Schiff base nitrogen into a hydrophobic region. This decreases the pK_a of the Schiff base by the order of 5 pK_a units, an approximate value which stems from the observation that the pK_a of the Schiff base is reduced to 8.5 when Asp85 is replaced by a neutral residue [106], which could be expected to disrupt the very same salt bridge between the Schiff base and Asp85. A very similar value for the pK_a of the Schiff base at its reprotonation step was determined from kinetic studies of the D96N mutant [107]. In the ground state structure, the low pK_a of 2.2 of Asp85 is stabilized by H-bonds to two water molecules (Wat401 and Wat402) and to Thr89 (Fig. 3), all of which act as H-bond donors to the negatively charged carboxylate. The loss of a H-bond to Wat402 in K_{110K} (Fig. 6A) increases the pK_a of Asp85 [26], and this value is further increased in L_{170K} by the loss of H-bonds to Wat401 and Thr89 (Fig. 6C) [27]. Nevertheless, one water molecule (Wat451, Fig. 8), which reorders between the two negatively charged aspartates, is still able to act as a proton donor to the carboxylate of Asp85. Because of the reversal of the orientation of the Schiff base nitrogen due to retinal isomerization, this positively charged group no longer compensates the negative charge on Asp212. In addition, by L_{LT} the positively charged guanidinium group of Arg82 has reoriented towards the extracellular medium (Figs. 6C,D and 8). Indeed, the movement of Arg82 facilitates a local flex of helix C [27] which exaggerates the interactions between the negatively charged Asp85 and Asp212, and also brings the backbone carbonyl oxygen of Arg82 into a position where it competes with Asp85 as a H-bond acceptor from Wat451 (Fig. 8). That the orientation of Arg82 has a dramatic effect on the pK_a of Asp85 is reflected by the fact that its replacement with a neutral residue (glutamine or alanine) increases the pK_a of Asp85 by 4.6 units [108–110]. Furthermore, for the R82H mutant at low pH (at which His is likely to be protonated) proton transfer from the Schiff base to Asp85 is almost entirely suppressed, yet the proton-transfer kinetics become similar to wild-type bR at high pH [111]. The combined effect of all these structural rearrangements is to raise the pK_a of Asp85 to the point where it becomes a proton acceptor relative to the Schiff base. Braiman et al. [112] have estimated that the pK_a of Asp85 reaches a value as high as 10.5 during the photocycle, which would be sufficient to reverse the proton donor/acceptor relationship of this group with respect to the lowered pK_a of the isomerized Schiff base.

Proton exchange between the Schiff base and Asp85 requires the existence of a low barrier pathway. This may

be facilitated by H-bonds to a water molecule [28], to Thr89 [33], or by direct proton transfer from the Schiff base to Asp85 [85]. In a recent review, Kandori [103] argued that FTIR spectroscopy studies appear consistent with either water-mediated or direct proton transfer. Nevertheless, the remarkable fact that the decay of the K-intermediate is six decades slower than its build-up, and that the K-to-L transition is associated with a local bend of helix C (Fig. 6C), strongly implies that this local perturbation of a secondary structural element is a crucial factor in redefining a pathway for proton transfer. This is further supported by the fact that the primary proton transfer occurs 10 times more rapidly in the D85E mutant [113], which would require smaller structural rearrangements to facilitate direct proton transfer. From this basis we postulated that the observed movement of Asp85 towards the Schiff base, which is exaggerated by this local bend of helix C (Fig. 6B,C), facilitates a mechanism whereby a proton is transferred directly from the Schiff base to Asp85, and proton transfer is modulated by structural fluctuations of the retinal [85]. That structural fluctuations of the photoisomerized retinal could transiently create a low barrier pathway for proton transfer from the Schiff base to Asp85 provides a modern picture curiously resembling (yet distinct from) a previously postulated double-isomerization mechanism [114]. Proton transfer would cancel the mutual electrostatic attraction between the positively charged Schiff base and the negatively charged Asp85, and thereby enable strain on helix C, as well as strain on the retinal [102], to relax structurally and draw the two groups apart. A separation of the primary proton donor and acceptor would certainly contribute strongly to vectoriality of the proton pump bR [27,33,85,102], since the reverse proton transfer from Asp85 to the Schiff base would be hindered. Alternative mechanisms for both the primary proton transfer event and their contribution to vectoriality are reviewed in Section 5.

4.3. Structures for the M-intermediates of bR

At room temperature, the primary proton transfer event, which corresponds spectrally to the L-to-M transition, takes approximately 40 μ s. It is well established by time-resolved studies that a spectrally silent transition, from an early to a late M-intermediate (i.e. M_1 to M_2 , Fig. 2B), follows on the time scale of 350 μ s [23]. Furthermore, a series of studies on 2-D crystals of bR in projection have conclusively shown that a large-scale structural rearrangement is associated with this transition, which opens the proton translocation channel to the cytoplasm [24,54–61]. It has long been considered that structures of both the early and late M-intermediates would shed light on the mechanism by which the Schiff base switches its accessibility from the extracellular to the cytoplasmic side. Structural details elucidating a pathway for reprotonation of the Schiff base from Asp96 on the cytoplasmic side (Fig. 1) [28,31], and the nature of the

movements which open the proton translocation channel to the cytoplasmic medium [32,33], have indeed emerged.

X-ray structures of the M-intermediates of the D96N bR mutant [30], the E204Q bR mutant [31], and of wild-type bR [28,29] have all been reported. The trapping protocols used in these studies are described in Section 3. Only in the work of Sass et al. [28] was a difference Fourier map presented. On the extracellular half of bR, the observed structural rearrangements of these M-states are all in agreement, within the errors of the technique. While there are variations with respect to the exact coordinates, these indicate noise within the crystallographic data, limitations of the trapping protocols, and structural changes due to the E204Q mutation on the extracellular side [31]. As would be expected, the key structural rearrangements which were required to set the stage for proton transfer were also present shortly after proton transfer. For example, all structures of M showed similar rearrangements of water molecules and a similar change in the orientation of Arg82 as seen in L_{LT} (Fig. 8) [27]. One striking difference between the structures of L_{LT} and M concerns the local flex of α -helix C in L_{LT} , shown in Fig. 6C as paired negative and positive electron density peaks which extend more than a full turn. While the difference Fourier map of the M state reported by Sass et al. [28] showed paired electron density peaks near the backbone carbonyl oxygens of Arg82 and Tyr83, there were no such peaks on the backbone of Asp85. Unfortunately, no difference Fourier maps were presented by the other workers, but nevertheless Luecke et al. [30] emphasized the fact that no displacements of the main chain were evident in helices A to E in their late M-state structure. As such these structures of the M-intermediate appear to support our mechanistic postulate that the local flex of helix C, which exaggerates the approach of Asp85 towards the Schiff base immediately prior to proton transfer, could relax to some extent following proton transfer since the mutual electrostatic attraction of the two groups would be cancelled.

One interesting feature of the proton pumping mechanism is that, for wild-type bR and at physiological temperature and pH, the timing of proton release to the extracellular medium is roughly coincident with the primary proton transfer event [20]. Structural changes on the extracellular side of bR provide insight into how this occurs. Luecke et al. [30] argued that the observed reorientation of the guanidinium group of Arg82 would destabilize the proton release group, which consists of the dyad of Glu194 and Glu204 [21,22] and associated water molecules. While it seems certain that the movement of Arg82 makes a significant contribution to the mechanism of proton release, it was also emphasized by Luecke [62] that the proton release complex is well insulated from the aqueous medium and hence other structural rearrangements are also required. Some clues for these additional rearrangements, which mainly include partial disordering near the glutamate dyad, have been reported [27].

While there is good agreement with respect to the nature of the structural rearrangements which occur on the extracellular side of the protein, there have been conflicting suggestions regarding the timing of these occurrences. Luecke et al. [30,31] and Sass et al. [28] have postulated that the reorientation of Arg82 is triggered by the protonation of Asp85, yet the structure of L_{LT} (Figs. 6B–D and 8) shows that this rearrangement occurs prior to the primary proton transfer event [27,85]. Luecke et al. [30] argued that the loss of H-bonds from Asp85 to water molecules and to Thr89 would be sufficient to achieve proton transfer and generate the M_1 state. They further suggested that proton transfer to Asp85 would then trigger the reorientation of the guanidinium group of Arg82, thereby causing proton release to the extracellular medium, leading to the transition from the early M state to the late M state, and increasing the pK_a of Asp85 to the point where it could no longer reprotonate the Schiff base. This structural mechanism promotes the observed movement of the side chain of Arg82 as the central element of vectoriality in the proton pump bR, and hinges upon the coincidence in time of proton transfer and proton release. It is therefore difficult to reconcile this mechanism with the conclusions drawn by the same group from kinetic studies at different temperature, pH, and of specific mutants, that proton release is not directly linked to Schiff base deprotonation, and that the temporal coincidence between them under some conditions must be fortuitous [20]. Indeed, this structural mechanism was overturned shortly later by the same group when they observed that the reorientation of Arg82 had already occurred by the formation of M_1 [31]. In fact, proton release appears to occur slightly faster than proton transfer in wild-type bR at 278 K, significantly slower at 308 K, and much slower still at pH < 5 [20]. Furthermore, the apparent coupling between proton transfer and release is entirely removed in several mutants, such as: the D85E bR mutant for which proton transfer is accelerated 10-fold while proton release is delayed 2-fold [20,113], the R82N and R82Q bR mutants for which M-formation is very rapid yet proton release is considerably delayed [108–110], and the E204Q mutant for which proton release is again delayed [21]. Whereas titration experiments on the unphotolyzed ground state implied a coupling between proton transfer to Asp85 and proton release of approximately 5 pK_a units [100], this coupling was only 0.7 pK_a units in the photolyzed state at physiological pH and temperature [115]. This apparent discrepancy is explained by the structure of L_{LT} , since the extended network of H-bonds linking Asp85 via Arg82 to the postulated release group in the ground state [17,18] (Fig. 3), is entirely disrupted prior to proton transfer [27,85] (Fig. 8).

In the ground state of bR, the cytoplasmic side of the proton transport channel acts as hydrophobic plug, preventing the back diffusion of protons through the membrane. X-ray structures of the M-intermediates [28–31] provide insight into how this region allows the transport of a proton first from Asp96 to the Schiff base. As seen in Fig. 6A, a

movement of the backbone carbonyl oxygen of Lys216 was detected early on in the photocycle [26]. This early movement becomes exaggerated as the photocycle proceeds (Fig. 6D) [27,28,30], and may be interpreted as a local unwinding of helix G in the immediate vicinity of a π -bulge [18]. Sass et al. [28] and Luecke et al. [31] have shown that these movements provide sites for water molecules to order (Fig. 9) and thereby define a pathway for proton transfer from Asp96 almost as far as the Schiff base nitrogen. That the carbonyl oxygen of Lys216 becomes further hydrated during the photocycle was anticipated by Takei et al. [116] on the basis of FTIR spectroscopy studies at low temperature. One appealing aspect of this mechanism is that in the X-ray structure of the Ca^{2+} -ATPase [7], a similar unwinding of one transmembrane α -helix was observed. In that work, it was suggested that the local unwinding of an α -helix

provided sites for water molecules to bind, and thereby reduced the energy barrier for the removal of the water molecules which coordinate the Ca^{2+} ion which is transported across the membrane. Water molecules bound near the carbonyl oxygen of Lys216 (Fig. 9), however, cannot protonate the Schiff base directly and it is not unreasonable to suggest that, in bR, the partial disordering of a water molecule could provide the final link needed for the reprotonation step [28]. In this context, however, it should be noted that the structure of Sass et al. [28] includes a uniquely large number of water molecules at 2.3 Å resolution, and therefore some may be placed with more confidence than others.

Numerous low-resolution 2-D studies of bR in projection have firmly established that the late M-state of the bR photocycle is associated with a major structural rearrange-

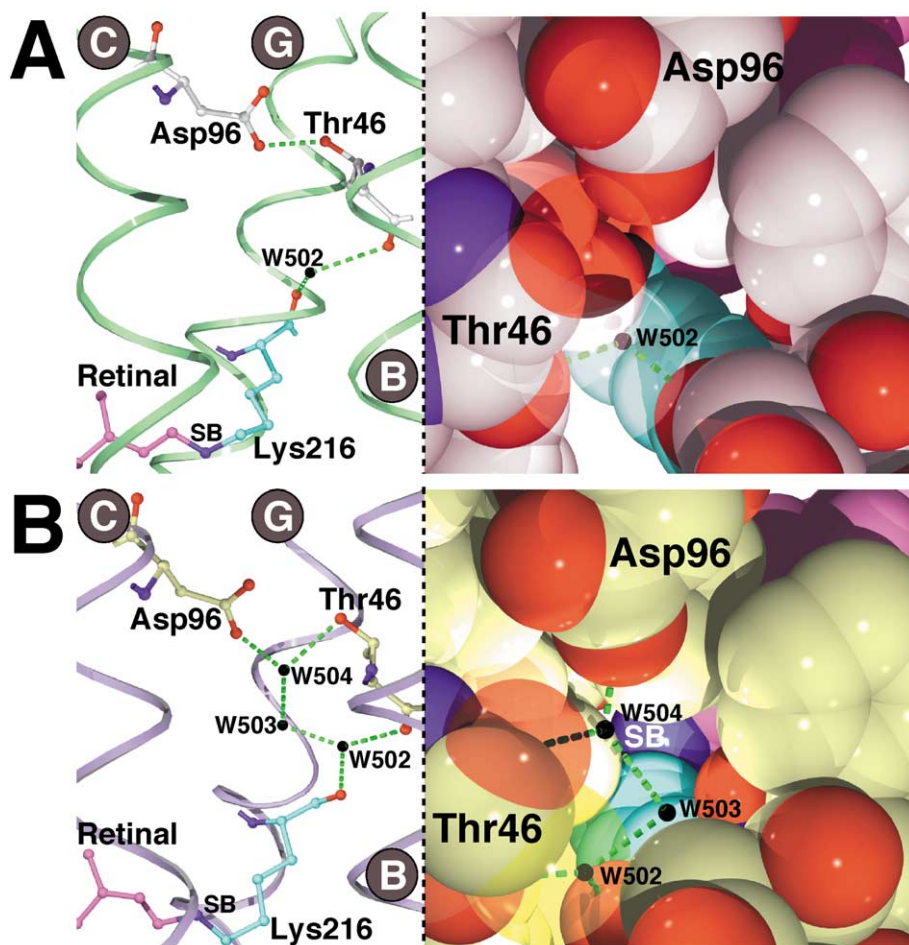


Fig. 9. Structural changes associated with the early M state of the E204Q bR mutant. (A) Structure of the E204Q bR mutant in the ground state, illustrating the proton translocation channel on the cytoplasmic side of the retinal. When the proton translocation channel is viewed from Asp96 towards the retinal (space filling model) the side chain of Lys216 is visible (cyan) but the Schiff base is occluded, showing the lack of accessibility to the cytoplasmic side in the ground state. (B) Structure of the early M intermediate of the E204Q bR mutant. Light-activated structural rearrangements allow two new water molecules (Wat503 and Wat504) to order along the proton translocation channel and define a network of H-bonds stretching from Asp96 to Lys216. The space filling model illustrates that when the proton translocation channel is viewed from Asp96 towards the retinal, the Schiff base (SB) nitrogen is visible (blue), indicating accessibility to the cytoplasmic side. Structural models are available from entries 1F4Z and 1F50 of the protein data bank. Details are found in Ref. [31]. This figure was drawn using the Swiss PDB Viewer [132].

ment of the cytoplasmic portions of helices E, F and G [24,54–61]. Thus, the publication of a high-resolution X-ray structure of the late M-intermediate of bR was eagerly awaited, since it was anticipated that this would provide a detailed 3-D structural model of this major conformational change. Fig. 10A superimposes upon the 1.9 Å model for ground state bR (green) [17] C α -traces of all published X-ray structures of the M-intermediate available in the protein data bank to date (except for the very recent structure of the M-state of Facciotti et al. [29], which had not been released when this review was being prepared): blue is the early M of the E204Q bR mutant [31]; red is the late M of the D96N bR mutant [30]; and gray is the late M of wild-type bR [28]. The structure shown in yellow is the 3-D electron diffraction structure of the D96G/F171C/F219L triple mutant in the

ground state, for which the cytoplasmic channel is constitutively open [33].

The first published structure for M, that of the D96N mutant [30] provided no insight as to the nature of these movements since the major portions of the cytoplasmic halves of helix E, F and G were entirely removed from the model (Fig. 10A, red) due to disordering of the electron density. In this context, a suggestive feature of this late M-state structure was the presence of a significant movement of the side chain of Trp182 arising from a steric clash with the C₁₃ methyl group of the isomerized retinal (Fig. 10A, red). This movement would exert a force upon helix F, and was previously suggested to provide a mechanism for driving an outwards tilt of the cytoplasmic half of this helix hinged near Pro186 [57]. In addition, the loss of electrostatic

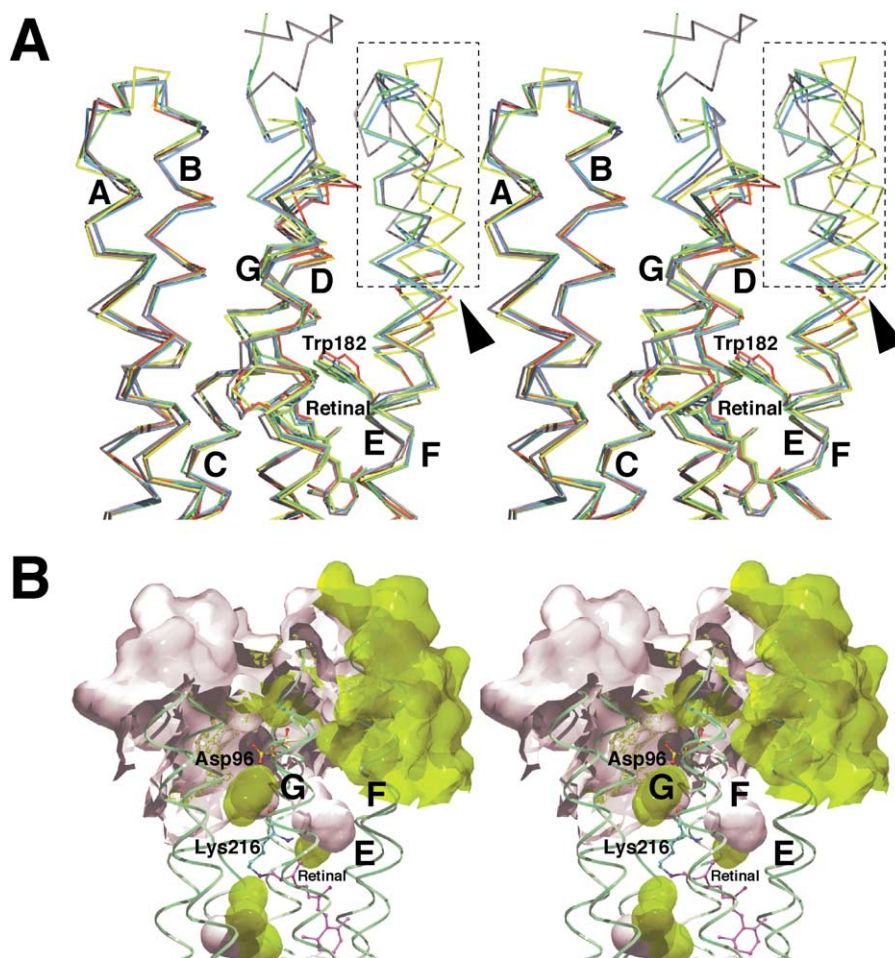


Fig. 10. Structural rearrangements on the cytoplasmic half of bR associated with the M-intermediates. (A) Superposition of C α traces of the early M of the E204Q bR mutant (blue, entry 1F4Z in the protein data bank); the late M of the D96N bR mutant (red, entry 1C8S); the M of wild-type bR (gray, entry 1CWQ); and the ground state of the D96G/F171C/F219L bR mutant (yellow, entry 1FBK), overlaid on the ground state model for wild-type bR (green, entry 1qhj). Only minor structural rearrangements are visible in the M-state structures of wild-type bR and the E204Q bR mutants, although the former structure departs significantly from all other models near the E–F loop. Large conformational changes are visible for helices E, F and G of the bR triple mutant. Significant disordering of the electron density for the D96N bR mutant caused large regions of the cytoplasmic halves of helices E, F and G to be removed from the model (highlighted using a black arrowhead). (B) Representation of the cytoplasmic surface and buried cavities of the ground state of bR (white) and that of the D96G/F171C/F219L triple mutant (yellow). The conformational change opens the protein to the cytoplasm near the interface of helices E and F with D and G. This surface also appears to stretch towards Asp96 at the interface of helices B, C and G. This figure was drawn using the Swiss PDB Viewer [132].

attraction between the Schiff base and Asp85 following proton transfer makes a significant contribution in achieving an open conformation for bR [92]. Luecke et al. [30] sought to overturn this mechanism on the basis of their D96N M-state structure [62] claiming that if any such concerted movement of helix F did occur it must originate from Val177. Shortly thereafter, the same authors published a structure for the early M of the E204Q bR mutant [31]. As described above, this structure (as with that of Sass et al. [28]) reported a number of water molecules which order between Lys216 and Asp96 during the photocycle (Fig. 9) and are therefore important in understanding the Schiff base reprotonation step. In addition, this structure was suggestive of the initial stages of an outwards tilt of helix F (Fig. 10A, blue), although the amplitude of the movements was relatively small, reaching around 0.7 Å near the cytoplasm. Sass et al. [28] observed a very similar movement for most of helix F (Fig. 10A, gray). However, this late M-state structure [28] diverges markedly from all other structures of bR near the cytoplasmic ends of helices E and F, and including the E–F loop. Due to the mixture of structural intermediates, relatively low occupancy and significant twinning, reservations regarding this structure have been raised [29,33]. Taken together, the X-ray results of the M intermediates to date present a puzzling picture as to the nature and extent of the movement of the cytoplasmic halves of helices E, F and G.

An electron diffraction structure to 3.2 (in the plane) and 3.6 (perpendicular) Å resolution, which shows the cytoplasmic half of the proton transport channel constitutively open was reported by Subramaniam and Henderson [33]. The key ingredient in this work was a comprehensive study of light-induced, and mutation-induced, structural changes of bR in projection which identified that the ground state of the D96G/F171C/F219L bR triple mutant shows the full extent of the light-induced structural changes in bR even without illumination [24]. Fig. 10A shows this structure (yellow) overlaid on the other X-ray models for M. An outwards tilt of helix F is evident, starting from Trp182, with the cytoplasmic end being displaced by approximately 3.5 Å, and the final turn of helix G being displaced approximately 2 Å towards the center of the protein. It is apparent that all X-ray structures for the M intermediates reported to date show (at best) only a fraction of this large-scale change in conformation. It has been suggested [62] that the crystal contacts between the BC loop of one molecule with the cytoplasmic surface of another molecule in the next layer of the 3-D crystal may provide an explanation as to why these movements are considerably hindered in 3-D crystals.

It is widely believed that a similar change in conformation is required to expose the cytoplasmic half of the proton translocation channel to the cytoplasm so as to aid the reprotonation of Asp96 (Fig. 1). In Fig. 10B the influence of this change in conformation on the proton translocation cavity is represented. The cytoplasmic surface and buried cavities are shown in white for the ground state of bR [17],

whereas the same are represented in yellow for the structure of the D96G/F171C/F219L bR mutant [33]. This representation illustrates how the model for the open conformation of bR derived from the bR triple mutant structure is considerably more exposed to the cytoplasmic medium at the interface of helices E and F with D and G, relative to the ground state structure. In addition, the surface of the triple mutant appears to stretch towards Asp96 near the interfaces of helices B and C. This feature is suggestive, since a negatively charged patch consisting of Asp36, Asp38, Asp102 and Asp104 is located at the cytoplasmic surface, and is thought to aid the reprotonation of Asp96 [117], but its mechanistic significance cannot be assigned with confidence. It has also been proposed that an opening of the cytoplasmic half of the protein might provide a mechanism whereby water molecules could enter the proton translocation channel from the cytoplasm [118], but the details of how this would occur are not clear from the structural model and no light-induced increase in the hydration of the M-state of the D96N mutant was detected by neutron diffraction [61]. In all probability, it is the combination of increased flexibility near the cytoplasmic surface, the free movement of disordered water molecules, as well as structural perturbations to the ground state H-bond formed between Asp96 and Thr46 (Fig. 9) [31], which combine to facilitate the reprotonation of Asp96 from the cytoplasmic medium. Both the nature of the structural rearrangements (Fig. 10) and the time scale required for this conformational change in wild-type bR (5 ms, Fig. 2B) suggest multiple pathways for this reprotonation step.

4.4. A structural model for the N-intermediate of bR

An electron diffraction study of the N-intermediate of the F219L bR mutant was reported to 3.5 Å in the horizontal and 5.5 Å in the vertical directions [32]. The intermediate was trapped by illumination for 30 s at 270 K. Difference Fourier analysis was used to illustrate that significant movements of helix F and G resulted from photoexcitation. Due to the intermediate resolution of the data, and the occupancy of the N-intermediate of only 20–30%, structural refinement was performed by refitting parts of the ground state structure as rigid bodies within the difference electron densities. The resulting model showed an outwards tilt of helix F, with the maximum displacement of around 3 Å near the E–F loop, and a smaller tilt of the cytoplasmic end of helix G towards the position originally occupied by helix F. A systematic study of light-induced structural changes of bR and several mutants in projection [24] has shown that the movements associated with the N intermediate have the same nature of those observed for the late M. While the 3-D model for the N-intermediate of the F219L mutant lacks the resolution of the other structures to date, it is in agreement with the structure of the open conformation of bR deriving from the D96G/F171C/F219L triple mutant (Fig. 10A), and hence adds weight to the suggestion that this accurately

models the large-scale conformational change of the bR photocycle [33].

Vonck [32] proposed that the large movement on the cytoplasmic side of helix F would induce a steric clash between one molecule of a trimer with another molecule of an adjacent trimer. As such an upper population of approximately one-third of all molecules would be able to adopt the open conformation simultaneously, and this was suggested to explain the relatively low occupancy of the trapped N-intermediate which was recovered. Moreover, it was suggested that it would not be possible to trap a 100% population of the open M₂ conformation in crystals of bR which maintained the trimer packing, even if it appeared from spectral analysis that close to 100% M was populated [62]. The argument was further extended to provide a basis for the so-called “cooperativity” effect whereby, at high illumination intensities, an increased proportion of a slowly decaying M-species builds up at the expense of a fast decaying species.

4.5. The O-intermediate

Following the reprotonation of the Schiff base from Asp96 (the M₂ to N transition), the propensity of the retinal to thermally re-isomerize to the all-*trans* configuration (Fig. 2) is greatly enhanced. This effect was demonstrated by Balashov et al. [100], who observed that the rate of dark adaptation is considerably slowed at very high pH, where the retinal is deprotonated. Steric effects within the retinal binding pocket also play a role in driving retinal reisomerization since the replacement of Leu93 (a residue near the retinal's C₁₃ methyl group, Fig. 2A) by an alanine [119] slows this step approximately 250-fold, and this kinetic defect is overcome in the presence of strong background illumination [120]. The reisomerization of the retinal back to the all-*trans* configuration, which characterizes the N-to-O transition, removes the steric clash of its C₁₃ methyl group with the side chain of Trp182, and thereby allows the open conformation of the cytoplasmic side of the protein to relax back to the ground state conformation. In addition, this step also removes a steric hindrance caused by the position of C_ε of Lys216 in the 13-*cis* configuration (Fig. 7) such that a water molecule (i.e. Wat402) could again accept a H-bond from the Schiff base (Fig. 3). The reordering of a water molecule at this key position would, in all probability, initiate the reordering of other water molecules on the extracellular side of the protein and facilitate the return of Arg82 back to its original conformation (Fig. 3). As such a pathway from Asp85 to the proton release group would again be established, and the lowered pK_a of Asp85 (due to the remaking of H-bonds which were disrupted in L) would drive the final proton transfer from Asp85 to the release group (Fig. 1) and thereby complete the photocycle.

Recently, an X-ray structure of the D85S bR mutant was reported [34]. This structure is interesting since the D85S bR mutant, like hR, pumps chloride ions from the extrac-

ellular medium to the cytoplasm. In contradistinction to the structure of hR [8], however, no bound chloride ions were observed. The structure of this mutant is quite similar to that of wild-type bR on the cytoplasmic side, but dramatically perturbed on the extracellular side. These perturbations are possibly responsible for the fact that this mutant crystallizes from the lipidic cubic phase in space group C222₁ rather than P6₃, which is the space group for lipidic cubic phase grown crystals of wild-type bR [40,41] and its D96N [30] and E204Q [31] mutants. Moreover, in crystals of the D85S bR mutant the molecules pack as dimers rather than trimers as in the purple membrane [17,35]. Rouhani et al. [34] argue that, since Asp85 is replaced with a neutral residue, this structure would provide a good model for the O-intermediate of the wild-type bR photocycle. This proposal is structurally and mechanistically questionable. The structure the D85S mutant showed changes of up to 3 Å for the extracellular sides of helices B, C, D and E, which open the proton transport channel to the extracellular (not the cytoplasmic) medium. No studies of the light-driven structural rearrangements in the bR photocycle support this conjecture. It was suggested that the neutralization of Asp85 would provide the driving force for these movements which would occur on a time scale of 20 ms (cf. Fig. 2B), yet the same group has shown that when light-driven proton transfer from the Schiff base neutralizes Asp85, no movements of helices A to D are detected even after a delay of 3 s at room temperature [30]. Instead, it was argued that a dramatic conformational change on the extracellular side of the protein is necessary so that a hydroxide ion may be taken up from the extracellular medium [34], which presents a major departure from the consensus picture as to how bR transports protons uphill against a proton-motive potential.

5. The primary proton transfer event and vectoriality of the pump

Structural results from X-ray crystallography represent an average over all conformations within the crystal. As such, when key steps along a catalytic mechanism are governed by transient fluctuations about the mean conformation they cannot be resolved directly. Unfortunately the movement of a proton between two groups falls into this category and hence subtle, yet potentially important, structural details may not be resolvable. For example, twisting motions of the retinal or the transient ordering of otherwise disordered water molecules may play important roles in the exchange of a proton between key groups. For these reasons, it is not unreasonable to anticipate that molecular dynamics [121] and quantum mechanical [122] simulations may ultimately prove decisive when choosing between conflicting models for the primary proton transfer event. The balance of evidence, nevertheless, favors some models over others.

Any model for the primary proton transfer event must simultaneously fulfill two criteria: Asp85 must become a proton acceptor relative to the Schiff base; and there must exist a low-barrier pathway along which a proton can be transferred. The high-resolution ground state structure of bR exhibits a short chain of H-bonds which link the Schiff base to Asp85 via Wat402 (Fig. 3), yet proton exchange does not occur due to the large pK_a difference between the two groups. As such, the structure of the active site in the ground state stabilizes an inactive, resting conformation. X-ray structures of K [26], L [27] and M [28–31] have produced a consensus picture as to the specific nature of the structural rearrangements which lower the pK_a of the Schiff base and increase that of Asp85, and these were described in detail in Section 4.2. As mentioned in Section 4.3, the only significant difference of opinion concerns the timing of the observed movement of the guanidinium group of Arg82 relative to the primary proton transfer event [28,30,31]. However, the combination of spectral (Fig. 5) and structural (Figs. 6B,C and 8) results shown here demonstrate that this conformational change occurs prior to proton transfer [27,85].

It is at first puzzling that, whereas the Schiff base N–H dipole is orientated favorably towards Asp85 in the ground state, photoisomerization about the $C_{13}=C_{14}$ double bond rotates it away from the proton acceptor and towards the cytoplasm (Figs. 2A and 6D) prior to proton transfer. An early model which explicitly addressed this enigma proposed that following the all-*trans* to 13-*cis* retinal isomerization, a second isomerization about the $C_{15}=N_{\zeta}$ bond occurs which would reorientate the Schiff base nitrogen and thereby redefine a transient pathway for direct proton transfer [114,123]. While the suggestion is appealing, this mechanism was later ruled out on the basis of resonance-Raman studies which showed that this second isomerization event did not occur [124].

In Section 4.2, we argued that structural fluctuations of the retinal, in particular twisting motions about the $C_{13}=C_{14}$, $C_{14}-C_{15}$ and $C_{15}=N_{\zeta}$ bonds, could be sufficient to transiently create a low-barrier pathway for direct proton transfer in L. Such fluctuations would be strongly influenced by the mutual electrostatic attraction of the Schiff base and Asp85, and specifically the fact that these two groups approach each other in L_{LT} (Fig. 6). Our model receives support from the fact that the primary proton transfer obeys single step kinetics [86], and from solid-state NMR studies [79,102] which established that Asp85 approaches a highly strained retinal in L_{LT} . One compelling argument which points towards direct proton transfer is the fact that the structural evolution from K_{LT} to L_{LT} is decisive in creating a proton transfer pathway, since no proton transfer occurred at 110 K [26] but did occur to a small extent at 170 K [27,85]. The observed movements were small but could, nevertheless, lower tremendously the height of energy barriers for direct proton exchange between the primary donor and acceptor. By the same argument, only

slight structural rearrangements following proton transfer would be needed to reinstate a large energy barrier, thus preventing the reprotonation of the Schiff base from Asp85. Proton transfer neutralizes these two groups and cancels their mutual electrostatic attraction, such that strain on the retinal [102] and locally on helix C [27] could relax and draw the proton donor and acceptor apart. Within this picture, the approach of Asp85 towards the Schiff base (which lowers the energy barrier of the primary proton transfer) and sequential retreat (which reinstates this barrier), as dictated by the protonation state of these two groups, provides the essence of vectoriality of the proton pump bR. A related mechanism, although not necessarily postulating direct proton transfer, has been termed “electrostatic steering” by Herzfeld and Tounge [102]. It was argued that if the breaking of the “electrostatic yoke” is efficient then the mechanism would be very tolerant of significant changes in the pH and other experimental conditions. It has also been suggested that retinal deprotonation itself decreases the curvature of the retinal [33], implying a complementary mechanism which also postulates an increased separation of the proton donor and acceptor as a consequence of proton transfer.

Another plausible mechanism for the proton transfer pathway was advocated by Sass et al. [28] who argued that a disordered water molecule (perhaps Wat402) could transiently define a pathway from the Schiff base to Asp85. The appeal of this mechanism is the fact that, if there are disordered water molecules in the immediate vicinity of these two groups, it is reasonable to expect that they would serve as “proton wires” mediating the proton exchange. As reviewed by Kandori [103], FTIR spectroscopy results appear to be consistent with either direct proton transfer or water-mediated proton transfer. While the observation of an ordered water molecule at a suitable position in L_{LT} would opt in favor of this mechanism, the fact that no such water molecule was observed (Fig. 8) does not necessarily rule it out. However, the structures of both K_{LT} and L_{LT} (Fig. 6) show that Asp85 crowds in towards the retinal, and hence steric considerations seem to point against this mechanism. A closely related mechanism was proposed by Subramaniam and Henderson [33] whereby the side chain oxygen of Thr89, rather than a transiently ordering water molecule, serves to provide a pathway for proton transfer. In this picture, the extent to which the retinal must twist so as to create a low-barrier proton transfer pathway from the Schiff base to Thr89 is much reduced relative to that required for proton transfer directly to Asp85. The observation that the replacement of Thr89 with Val did not slow the primary proton transfer step weighs against this suggestion [86]. Nevertheless, support for this pathway is provided by a recent FTIR study which indicated that the H-bond between O_{δ} of Thr89 and $O_{\delta 2}$ of Asp85 is stronger in K, L and M than in the ground state [82]. These conclusions, however, are in conflict with all X-ray structures of the photocycle intermediates which consistently show this H-bond to be

substantially weakened (Figs. 6C and 8) [26–31]. A resolution of this apparent disagreement between the FTIR spectroscopy and X-ray results may have to await a more detailed theoretical treatment of the calculated IR spectra, since Hayashi and Ohmine [125] have shown, using ab initio quantum mechanical and molecular mechanics methods, that electronic interactions and polarization effects are important when describing the vibrational structure. Since the retinal isomerization reverses the orientation of the Schiff base dipole and greatly perturbs its interaction with both Thr89 and Asp85, this may influence the interpretation of FTIR spectra.

The models involving water-mediated or Thr89-mediated proton transfer share the feature that the postulated proton-transfer pathway would appear to be equally well defined, and rather similar, in both K_{LT} and L_{LT} . This therefore raises the question as to why subtle movements of a fraction of an angstrom from K_{LT} to L_{LT} (Fig. 6D) are decisive in setting the stage for proton transfer. Similarly, it is not obvious from either picture how structural changes immediately following proton transfer would hinder the reprotonation of the Schiff base from Asp85. A proposed straightening of the retinal [33] would displace the Schiff base away from Asp85, but this effect is much reduced relative to Thr89. A further puzzle arising from both pictures concerns the time scale for the primary proton transfer event, which is 40 μ s (Fig. 2B). This appears to be unreasonably slow should the primary proton transfer proceed via water or Thr89-mediated “proton wires” since either pathway would, in all likelihood, become defined shortly following retinal isomerization. This time scale poses no problem within our mechanism for direct proton transfer, however, since the time required for a local bend of helix C to occur would be of the order of microseconds, and this movement is required to exaggerate the early approach of Asp85 towards the Schiff base (Fig. 6). Nevertheless, at this time this issue is not definitively settled, and it is hoped that imaginative experiments or simulations will eventually lead to a conclusive mechanism of primary proton transfer in bR.

As reviewed by Stoeckenius [126], the discovery of the chloride pump hR briefly revived an earlier discussion as to whether bR pumps hydroxide ions towards the cytoplasmic side, rather than protons towards the extracellular side. At the time, no plausible mechanism for OH^- transport was proposed and the idea was soon abandoned. The availability of a high-resolution X-ray structure of hR has breathed new life into this old debate. Kolbe et al. [8] observed a Cl^- ion bound on the extracellular side of the Schiff base nitrogen of hR in a position analogous to that of O δ 2 of Asp85 in bR. This observation was the basis for proposing that the reversal of the orientation of the Schiff base dipole moment upon photoisomerization about the $\text{C}_{13}=\text{C}_{14}$ bond would provide the driving force for vectorial chloride transport towards the cytoplasmic side in hR. Luecke et al. [30,34,62,88] have recently argued that a similar mecha-

nism may also hold for OH^- transport in bR. Within this picture, it is proposed that retinal isomerization alone is sufficient to elevate the $\text{p}K_a$ of Asp85 from 2.2 to the point where it abstracts a proton from the neighboring Wat402, thereby creating a mobile hydroxide ion [62]. This postulate is doubtful, as it is unclear why a proton would not also be abstracted from Wat402 following dark adaptation (i.e. thermal isomerization about the $\text{C}_{15}=\text{N}_\zeta$ bond [100]). The creation of a negatively charged hydroxide in very close proximity to the Schiff base would greatly enhance the Schiff base–counter ion interaction and consequently a strong blue shift in the absorption spectrum would be expected [104]. The K-intermediate, however, is red-shifted relative to the ground state. According to the mechanism, this hydroxide ion would then be repelled by Asp212 and attracted by the Schiff base, thereby migrating towards the cytoplasmic side of the retinal where it would accept a proton from the Schiff base nitrogen [62]. It is puzzling, given the strength of the electrostatic driving force, why a time scale of 40 μ s would be necessary for the hydroxide ion to migrate a distance of approximately 4 \AA (mean velocity $\sim 10^{-5}$ m/s; the average thermal velocity of a water molecule at room temperature is $\sim 10^3$ m/s). No explanation of the blue shift associated with the K-to-L spectral transition is offered, nor do other structural rearrangements such as the reorientation of water molecules and the side chain of Arg82 play any obvious role [27–31]. This mechanism has recently been extended to suggest that a large-scale rearrangement of the extracellular side of bR, which results from the mutation of Asp85 to Ser, also occurs late in the bR photocycle and enables a hydroxide ion to be taken up from the extracellular medium [34]. This structural argument is not supported by any studies on photoactivated bR. For these reasons the proposed hydroxide pumping mechanism appears unlikely to gain widespread support.

6. Overview of the structural mechanism

Prior to the availability of high-resolution structures of bR in its ground and photocycle intermediate states, which provide exquisite details on its structural evolution, the mechanism of vectorial proton transport in bR was sketched in general terms. Frequently cited frameworks include the isomerization/switch/transfer (IST) model [127] and the local access model [128]. All emphasized the fact that structural details in the vicinity of the retinal must first define a pathway for proton transfer from the Schiff base to Asp85 on the extracellular side of the protein. Further structural rearrangements then break the accessibility to Asp85 and create a pathway for proton transfer from Asp96 on the cytoplasmic side of the protein back to the Schiff base. The structural results reviewed here provide a detailed atomic picture of these events and are summarized schematically in Fig. 11.

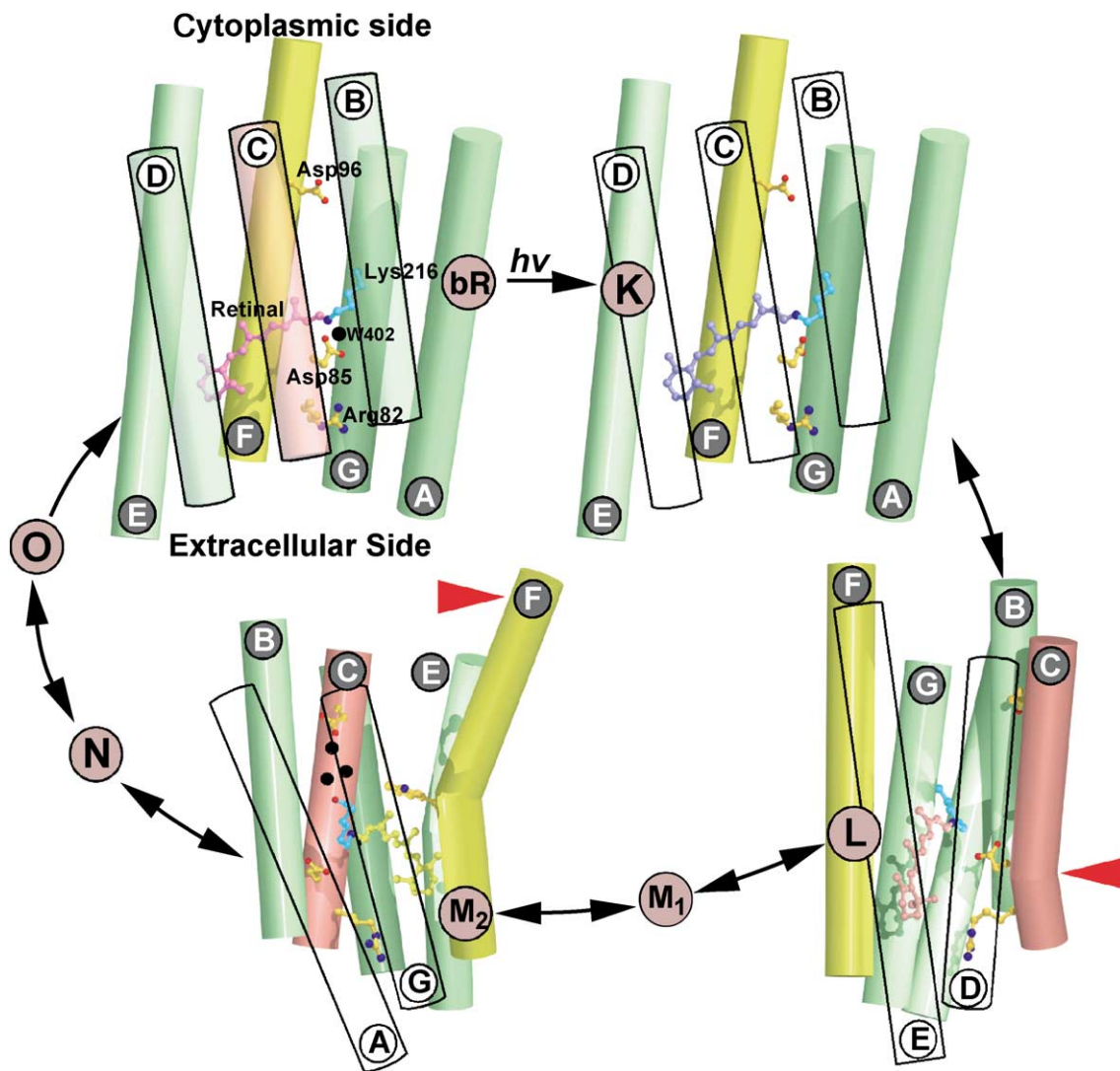


Fig. 11. Schematic overview of the mechanistically significant conformational changes which occur during the bR photocycle. In the ground state model (bR) the protonated Schiff base nitrogen (blue) is H-bonded to Wat402 (black), which is in turn H-bonded to Asp85. Following the photoisomerization of the retinal, the Schiff base N–H dipole reorients towards the cytoplasm and Wat402 becomes disordered (K), breaking the accessibility of the Schiff base to Asp85. A local flex of helix C (L, highlighted using a red arrowhead) allows Asp85 to approach the Schiff base, and the accessibility is transiently recreated enabling a proton to be transferred to Asp85. The reorientation of Arg82 towards the extracellular medium facilitates this bend of helix C, increases the pK_a of Asp85, and sets the stage for proton release to the extracellular medium. In M_2 water molecules (black) order along the cytoplasmic half of the proton translocation channel and an outwards movement of helix F (highlighted using a red arrowhead) exposes key groups to the cytoplasmic medium. These structural changes allow the Schiff base to be reprotonated from Asp96, and Asp96 to be reprotonated in turn from the cytoplasm. Structural relaxation recovers the original conformation, and a proton is transferred from Asp85 to the proton release group. For emphasis, helix C is colored red and helix F is colored yellow. This figure was drawn using a modified version of Bobscrip [130] and rendered using Raster3D [131]. Preparation of all structural figures was assisted using O [133]. An animation is available at www.csb.gu.se/neutze/movie.

In the ground state of bR, a hydrogen-bonded network consisting of polar residues and water molecules stabilizes the structure of the protein's extracellular half, connecting the Schiff base to the extracellular medium. Light-induced retinal isomerization about the $C_{13}=C_{14}$ bond reverses the orientation of the N–H dipole of the Schiff base, which in the ground state is H-bonded to Wat402. It also causes a steric clash between the C_ϵ of Lys216 (the residue to which the retinal is bound) and Wat402. This strategic water molecule, which plays a key role in stabilizing the resting

state, is consequently displaced, triggering a cascade of structural rearrangements on the extracellular side of bR. The network of water molecules becomes extensively disrupted and the guanidinium group of Arg82 reorients towards the extracellular medium. These changes dramatically perturb the pK_a values of key groups, and also facilitate a local flex of helix C which exaggerates an early movement of Asp85 towards the protonated Schiff base. This movement is driven in part by the mutual electrostatic attraction of the proton donor and acceptor, and the

approach of Asp85 towards the Schiff base creates a transient pathway for direct (or arguably indirect) proton transfer. Proton transfer then cancels this electrostatic attraction and releases strain on both the retinal and helix C, enabling the proton donor and acceptor to be drawn apart, thereby hindering the reversal of the proton transfer reaction. Proton release to the extracellular medium is assisted by the reorientation of the side chain of Arg82, as well as other movements which expose the proton release group to the extracellular surface. A number of events on the cytoplasmic side of the protein follow (see below), and the final proton transfer from Asp85 to the release group is delayed until the end of the photocycle, presumably occurring as the original network of water-mediated H-bonds on the extracellular side is restored.

The ground state structure of bR does not display an extended network of water molecules on the cytoplasmic side. Rather, the proton transport channel is characterized by an extended hydrophobic region which prevents the leakage of the stored proton-motive potential. Photoisomerization of the retinal results in a physical pulling on the side chain of Lys216 which induces, early on, a small movement of its main chain. This movement becomes exaggerated as the photocycle evolves, and a local unwinding of helix G in this region provides sites for water molecules to transiently order and thereby define a pathway for reprotonation from Asp96 almost as far as the Schiff base nitrogen. The final link facilitating Schiff base reprotonation from Asp96 is presumably provided by a disordered water molecule. A steric clash of the retinal's C₁₃ methyl group with Trp182 following retinal isomerization provides the driving force for an outwards tilt of the cytoplasmic half of helix F which evolves later in the photocycle. This is assisted by proton transfer since the electrostatic attraction of the Schiff base towards Asp85 and Asp212 is released. A large outwards movement of helix F opens the hydrophobic plug, enabling Asp96 to be reprotonated from the cytoplasm. Finally, once the retinal thermally reverts back to the all-*trans* configuration, the steric clash of the retinal's C₁₃ methyl group with Trp182 is removed and this allows the structure to relax back to the ground state conformation.

With most of the major steps of the photocycle now characterized structurally, bR should provide fertile ground for molecular dynamics and *ab initio* quantum mechanical simulations of the key events in the mechanism of this light-induced proton pump. Important issues which remain controversial concern the details of specific proton transfer events, and it would be valuable to recover reliable estimates for the pK_a changes of key groups during the photocycle. It should also be possible to experimentally test some of the major findings of the structural model, such as the transient loss and creation of H-bonds to key groups, or observe the local flex of the backbone of helix C, using time-resolved FTIR spectroscopy and other spectroscopic techniques.

Of particular interest is the extent to which the key ideas emerging from the structural picture can be generalized and applied to the understanding of other vectorial transport processes. Proton pumps such as cytochrome *c* oxidase [3] and ATP synthase [6] both contain proton translocation channels with an aspartate or glutamate located approximately halfway through the membrane. It is believed that, as with bR, water molecules play functional roles within the proton translocation channel of cytochrome *c* oxidase [129]. Other ion pumps such as Ca²⁺-ATPase [7] are expected to undergo large conformational changes in order to facilitate the translocation of ions. As such, it seems certain that the occurrence of both local and extended distortions of α -helices, side chain movements of charged groups, and the transient disordering and/or reordering of water molecules, will also feature within the structural mechanism of other systems. More subtle themes, such as the creation of strain due to the electrostatic attraction between oppositely charged groups and its consequent release following proton exchange, also appear sufficiently general to warrant further consideration in a wider mechanistic context.

Acknowledgements

We acknowledge the experimental support of C. Andersson, H. Belrhali, D. Bourgeois, A. Hardmeyer, P. Nollert and T. Ursby throughout this project. We thank J. Hajdu, R. Henderson, J. Herzfeld, H. Kandori, J.P. Rosenbusch, and G. Zaccai for discussions. Permission to reproduce data shown in Figs. 4 and 5 were given by G. Zaccai, and Photochemistry and Photobiology, respectively. Support from the Swedish Science Research Council (VR), SWEGENE, the Swedish Strategic Research Foundation (SSF), the French Ministry of Education and Research (MENR), the EU-Biotech, the Swiss National Science Foundation's SPP BIOTECH, the Welch Foundation, and the Howard Hughes Medical Institute is greatly acknowledged.

References

- [1] P. Mitchell, *Nature* 191 (1961) 144–148.
- [2] J. Deisenhofer, O. Epp, K. Miki, R. Huber, H. Michel, *Nature* 318 (1985) 618–624.
- [3] S. Iwata, C. Ostermeier, B. Ludwig, H. Michel, *Nature* 376 (1995) 660–669.
- [4] S. Iwata, J.W. Lee, K. Okada, J.K. Lee, M. Iwata, B. Rasmussen, T.A. Link, S. Ramaswamy, B.K. Jap, *Science* 281 (1998) 64–71.
- [5] M. Saraste, *Science* 283 (1999) 1488–1493.
- [6] D. Stock, A.G.W. Leslie, J.E. Walker, *Science* 286 (1999) 1700–1705.
- [7] C. Toyoshima, M. Nakasako, H. Nomura, H. Ogawa, *Nature* 405 (2000) 647–655.
- [8] M. Kolbe, H. Besir, L.-O. Essen, D. Oesterhelt, *Science* 288 (2000) 1390–1396.
- [9] W. Stoekenius, R.J. Rowen, *Cell Biol.* 34 (1967) 365–393.

- [10] D. Oesterhelt, W. Stoeckenius, *Nature New Biol.* 233 (1971) 149–152.
- [11] O. Béjà, L. Aravind, E.V. Koonin, M.T. Suzuki, A. Hadd, L.P. Nguyen, S.B. Jovanovich, C.M. Gates, R.A. Feldman, J.L. Spudich, E.N. Spudich, E.F. DeLong, *Science* 289 (2000) 1902–1906.
- [12] J.A. Bieszke, E.N. Spudich, K.L. Scott, K.A. Borkovich, J.L. Spudich, *Biochemistry* 38 (1999) 14138–14145.
- [13] D. Oesterhelt, *Curr. Opin. Struct. Biol.* 8 (1998) 489–500.
- [14] J.L. Spudich, *Mol. Microbiol.* 28 (1998) 1051–1058.
- [15] R. Henderson, J.M. Baldwin, T.A. Ceska, F. Zemlin, E. Beckmann, K.H. Downing, *J. Mol. Biol.* 213 (1990) 899–929.
- [16] L.-O. Essen, R. Siegert, W.D. Lehmann, D. Oesterhelt, *Proc. Natl. Acad. Sci. U. S. A.* 95 (1998) 11673–11678.
- [17] H. Belrhali, P. Nollert, A. Royant, C. Menzel, J.P. Rosenbusch, E.M. Landau, E. Pebay-Peyroula, *Structure* 7 (1999) 909–917.
- [18] H. Luecke, B. Schobert, H.T. Richter, J.-P. Cartiailler, J.K. Lanyi, *J. Mol. Biol.* 291 (1999) 889–900.
- [19] J. Lanyi, *J. Biol. Chem.* 272 (1997) 31209–31212.
- [20] Y. Cao, L.S. Brown, J. Sasaki, A. Maeda, R. Needleman, J.K. Lanyi, *Biophys. J.* 68 (1995) 1518–1530.
- [21] L.S. Brown, J. Sasaki, H. Kandori, A. Maeda, R. Needleman, J.K. Lanyi, *J. Biol. Chem.* 270 (1995) 27122–27126.
- [22] S.P. Balashov, E.S. Imasheva, T.G. Ebrey, N. Chen, D.R. Menick, R.K. Crouch, *Biochemistry* 36 (1997) 8671–8676.
- [23] B. Hessling, J. Herbst, R. Rammelsberg, K. Gerwert, *Biophys. J.* 73 (1997) 2071–2080.
- [24] S. Subramaniam, M. Lindahl, P. Bullough, A.R. Faruqi, J. Tittor, D. Oesterhelt, L. Brown, J. Lanyi, R. Henderson, *J. Mol. Biol.* 287 (1999) 145–161.
- [25] A. Miller, D. Oesterhelt, *Biochim. Biophys. Acta* 1020 (1990) 57–64.
- [26] K. Edman, P. Nollert, A. Royant, H. Belrhali, E. Pebay-Peyroula, J. Hajdu, R. Neutze, E.M. Landau, *Nature* 401 (1999) 822–826.
- [27] A. Royant, K. Edman, T. Ursby, E. Pebay-Peyroula, E.M. Landau, R. Neutze, *Nature* 406 (2000) 645–648.
- [28] H.J. Sass, G. Büldt, R. Gessenich, D. Hehn, D. Neff, R. Schlesinger, J. Berendzen, P. Ormos, *Nature* 406 (2000) 649–653.
- [29] M.T. Facciotti, S. Rouhani, F.T. Burkard, F.M. Betancourt, K.H. Downing, R.B. Rose, G. McDermott, R.M. Glaeser, *Biophys. J.* 81 (2001) 3442–3455.
- [30] H. Luecke, B. Schobert, H.T. Richter, J.-P. Cartiailler, J.K. Lanyi, *Science* 286 (1999) 255–260.
- [31] H. Luecke, B. Schobert, J.-P. Cartiailler, H.-T. Richter, A. Rosengarth, R. Needleman, J.K. Lanyi, *J. Mol. Biol.* 300 (2000) 1237–1255.
- [32] J. Vonck, *EMBO J.* 19 (2000) 2152–2160.
- [33] S. Subramaniam, R. Henderson, *Nature* 406 (2000) 653–657.
- [34] S. Rouhani, J.-P. Cartiailler, M.T. Facciotti, P. Walian, R. Needleman, J.K. Lanyi, R.M. Glaeser, H. Luecke, *J. Mol. Biol.* 313 (2001) 615–628.
- [35] R. Henderson, P.N.T. Unwin, *Nature* 257 (1975) 28–32.
- [36] N. Grigorieff, T.A. Ceska, K.H. Downing, J.M. Baldwin, R. Henderson, *J. Mol. Biol.* 259 (1996) 393–421.
- [37] Y. Kimura, D.G. Vassilyev, A. Miyazawa, A. Kidera, M. Matsushima, K. Mitsuoka, K. Murata, T. Hirai, Y. Fujiyoshi, *Nature* 389 (1997) 206–211.
- [38] K. Mitsuoka, T. Hirai, K. Murata, A. Miyazawa, A. Kidera, Y. Kimura, Y. Fujiyoshi, *J. Mol. Biol.* 286 (1999) 861–882.
- [39] H. Michel, D. Oesterhelt, *Proc. Natl. Acad. Sci. U. S. A.* 77 (1980) 1283–1285.
- [40] E.M. Landau, J.P. Rosenbusch, *Proc. Natl. Acad. Sci.* 93 (1996) 14532–14535.
- [41] E. Pebay-Peyroula, G. Rummel, J.P. Rosenbusch, E.M. Landau, *Science* 277 (1997) 1676–1681.
- [42] G. Rummel, A. Hardmeyer, C. Widmer, M.L. Chiu, P. Nollert, K.P. Locher, I. Pedruzzi, E.M. Landau, J.P. Rosenbusch, *J. Struct. Biol.* 121 (1998) 82–91.
- [43] P. Nollert, A. Royant, E. Pebay-Peyroula, E.M. Landau, *FEBS Lett.* 457 (1999) 205–208.
- [44] M.L. Chiu, P. Nollert, M.C. Loewen, H. Belrhali, E. Pebay-Peyroula, J.P. Rosenbusch, E.M. Landau, *Acta Crystallogr., D* 56 (2000) 781–784.
- [45] E. Pebay-Peyroula, R. Neutze, E.M. Landau, *Biochim. Biophys. Acta* 1460 (2000) 119–132.
- [46] P. Nollert, H. Qiu, M. Caffrey, J.P. Rosenbusch, E.M. Landau, *FEBS Lett.* 504 (2001) 179–186.
- [47] H. Sato, K. Takeda, T. Hino, T. Okada, M. Nakasako, N. Kamiya, T. Kouyama, *Acta Crystallogr., D* 56 (1999) 1251–1256.
- [48] A. Royant, P. Nollert, K. Edman, R. Neutze, E.M. Landau, E. Pebay-Peyroula, J. Navarro, *Proc. Natl. Acad. Sci. U. S. A.* 98 (2001) 10131–10136.
- [49] H. Luecke, B. Schobert, J.K. Lanyi, E.N. Spudich, J.L. Spudich, *Science* 293 (2001) 1499–1503.
- [50] M. Sheves, A. Albeck, N. Friedman, M. Ottolenghi, *Proc. Natl. Acad. Sci. U. S. A.* 83 (1986) 3262–3266.
- [51] C.H. Chang, R. Jonas, R. Govindjee, T.G. Ebrey, *Photochem. Photobiol.* 47 (1988) 261–265.
- [52] Y. Gat, M. Sheves, *J. Am. Chem. Soc.* 115 (1993) 3772–3773.
- [53] V. Reat, H. Patzelt, M. Ferrand, C. Pfister, D. Oesterhelt, G. Zaccai, *Proc. Natl. Acad. Sci. U. S. A.* 95 (1998) 4970–4975.
- [54] N.A. Dencher, D. Dresselhaus, G. Zaccai, G. Büldt, *Proc. Natl. Acad. Sci. U. S. A.* 86 (1989) 7876–7879.
- [55] M.H. Koch, N.A. Dencher, D. Oesterhelt, H.J. Plohn, G. Rapp, G. Büldt, *EMBO J.* 10 (1991) 521–526.
- [56] M. Nakasako, M. Kataoka, Y. Amemiya, F. Tokunaga, *FEBS Lett.* 292 (1991) 73–75.
- [57] S. Subramaniam, M. Gerstein, D. Oesterhelt, R. Henderson, *EMBO J.* 12 (1993) 1–8.
- [58] B.G. Han, J. Vonck, R.M. Glaeser, *Biophys. J.* 67 (1994) 1179–1186.
- [59] J. Vonck, *Biochemistry* 35 (1996) 5870–5878.
- [60] H.J. Sass, I.W. Schachowa, G. Rapp, M.H.J. Koch, D. Oesterhelt, N.A. Dencher, G. Büldt, *EMBO J.* 16 (1997) 1484–1491.
- [61] M. Weik, G. Zaccai, N.A. Dencher, D. Oesterhelt, T. Hauss, *J. Mol. Biol.* 275 (1998) 625–634.
- [62] H. Luecke, *Biochim. Biophys. Acta* 1460 (2000) 133–156.
- [63] J. Hajdu, I. Andersson, *Annu. Rev. Biophys. Biomol. Struct.* 22 (1993) 467–498.
- [64] J. Heberle, G. Büldt, E. Koglin, J.P. Rosenbusch, E.M. Landau, *J. Mol. Biol.* 281 (1998) 587–592.
- [65] I. Schlichting, J. Berendzen, G.N. Phillips Jr., R.M. Sweet, *Nature* 371 (1994) 808–812.
- [66] U.K. Genick, G.E. Borgstahl, K. Ng, Z. Ren, C. Pradervand, P.M. Burke, V. Srajer, T.Y. Teng, W. Schildkamp, D.E. McRee, K. Moffat, E.D. Getzoff, *Science* 275 (1997) 1471–1475.
- [67] U.K. Genick, S.M. Soltis, P. Kuhn, I.L. Canestrelli, E.D. Getzoff, *Nature* 392 (1998) 206–209.
- [68] K. Chu, J. Vojtechovsky, B.H. McMahon, R.M. Sweet, J. Berendzen, I. Schlichting, *Nature* 403 (2000) 921–923.
- [69] M.H.B. Stowell, T.M. McPhillips, D.C. Rees, S.M. Soltis, E. Abresch, G. Feher, *Science* 276 (1997) 812–816.
- [70] V. Srajer, T.Y. Teng, T. Ursby, C. Pradervand, Z. Ren, S.I. Adachi, W. Schildkamp, D. Bourgeois, M. Wulff, K. Moffat, *Science* 274 (1996) 1726–1729.
- [71] B. Perman, V. Srajer, R. Zhong, T. Tsu-Yi, C. Pradervand, T. Ursby, D. Bourgeois, F. Schotte, M. Wulff, R. Kort, K. Hellingwerf, K. Moffat, *Science* 279 (1998) 1946–1950.
- [72] P. Ormos, *Proc. Natl. Acad. Sci. U. S. A.* 88 (1991) 473–477.
- [73] A. Xie, *Biophys. J.* 58 (1990) 1127–1132.
- [74] S.P. Balashov, E.S. Imasheva, R. Govindjee, T.G. Ebrey, *Photochem. Photobiol.* 54 (1991) 955–961.
- [75] P.A. Bullough, R. Henderson, *J. Mol. Biol.* 286 (1999) 1663–1671.
- [76] B. Becher, F. Tokunaga, T.G. Ebrey, *Biochemistry* 17 (1978) 2293–2300.
- [77] A. Maeda, J. Sasaki, Y. Yamazaki, R. Needleman, J.K. Lanyi, *Biochemistry* 33 (1994) 1713–1717.
- [78] A. Maeda, H. Kandori, Y. Yamazaki, S. Nishimura, M. Hatanaka,

- Y.-S. Chon, J. Sasaki, R. Needleman, J.K. Lanyi, *J. Biochem.* 121 (1997) 399–406.
- [79] J.G. Hu, B.Q. Sun, A.T. Petkova, R.G. Griffin, J. Herzfeld, *Biochemistry* 36 (1997) 9316–9322.
- [80] M.S. Braiman, T. Mogi, T. Marti, L.J. Stern, H.G. Khorana, K.J. Rothschild, *Biochemistry* 27 (1998) 8516–8520.
- [81] F.M. Hendrickson, F. Burkard, R.M. Glaeser, *Biophys. J.* 75 (1998) 1446–1454.
- [82] H. Kandori, Y. Yamazaki, Y. Shichida, J. Raap, J. Lugtenburg, M. Belenky, J. Herzfeld, *Proc. Natl. Acad. Sci.* 98 (2001) 1571–1576.
- [83] S.P. Balashov, F.F. Litvin, V.A. Sineshchekov, in: V.P. Skulachev (Ed.), *Physicochemical Biology Reviews*, vol. 8. Harwood Academic Publishers, UK, 1988, pp. 1–61.
- [84] A. Hadfield, J. Hajdu, *J. Appl. Crystallogr.* 26 (1993) 839–842.
- [85] A. Royant, K. Edman, T. Ursby, E. Pebay-Peyroula, E.M. Landau, R. Neutze, *Photochem. Photobiol.* 74 (2001) 794–804.
- [86] J.K. Lanyi, *J. Phys. Chem., B* 104 (2000) 11441–11448.
- [87] S.P. Balashov, T.G. Ebrey, *Photochem. Photobiol.* 73 (2001) 453–462.
- [88] J.K. Lanyi, H. Luecke, *Curr. Opin. Struct. Biol.* 11 (2001) 415–419.
- [89] K. Ng, E.D. Getzoff, K. Moffat, *Biochemistry* 34 (1995) 879–890.
- [90] A. Mozzarelli, G.L. Rossi, *Annu. Rev. Biophys. Biomol. Struct.* 25 (1996) 343–365.
- [91] A. Xie, L. Kelemen, J. Hendricks, B.J. White, K.J. Hellingwerf, W.D. Hoff, *Biochemistry* 40 (2001) 1510–1517.
- [92] L.S. Brown, H. Kamikubo, L. Zimanyi, M. Kataoka, F. Tokunaga, P. Verdegem, J. Lugtenburg, J.K. Lanyi, *Proc. Natl. Acad. Sci. U. S. A.* 94 (1997) 5040–5044.
- [93] J. Sasaki, L.S. Brown, Y.S. Chon, H. Kandori, A. Maeda, R. Needleman, J.K. Lanyi, *Science* 269 (1995) 73–75.
- [94] W. Kühlbrandt, *Nature* 406 (2000) 569–570.
- [95] M. Braiman, R. Mathies, *Proc. Natl. Acad. Sci. U. S. A.* 79 (1988) 403–407.
- [96] J.S. Doig, P.J. Reid, R.A. Mathies, *J. Phys. Chem.* 95 (1991) 6372–6379.
- [97] R. Henderson, J.K. Moffat, *Acta Crystallogr., B* 27 (1971) 1414–1420.
- [98] Q. Song, G.S. Harms, C. Wan, C.K. Johnson, *Biochemistry* 33 (1994) 14026–14033.
- [99] H. Kandori, K. Shimono, Y. Sudo, M. Iwamoto, Y. Shichida, N. Kamo, *Biochemistry* 40 (2001) 9238–9246.
- [100] S.P. Balashov, E.S. Imasheva, R. Govindjee, T.G. Ebrey, *Biophys. J.* 70 (1996) 473–481.
- [101] H.G. Khorana, *Proc. Natl. Acad. Sci. U. S. A.* 90 (1993) 1166–1171.
- [102] J. Herzfeld, B. Tounge, *Biochim. Biophys. Acta* 1460 (2000) 95–105.
- [103] H. Kandori, *Biochim. Biophys. Acta* 1460 (2000) 177–191.
- [104] A. Albeck, N. Livnah, H. Gottlieb, M. Sheves, *J. Am. Chem. Soc.* 114 (1992) 2400–2411.
- [105] L. Ren, C.H. Martin, K.J. Wise, N.B. Gillespie, H. Luecke, J.K. Lanyi, J.L. Spudich, R.R. Birge, *Biochemistry* 40 (2001) 13906–13914.
- [106] T. Marti, S. Rossetlet, H. Otto, M. Heyn, H.G. Khorana, *J. Biol. Chem.* 266 (1991) 18674–18683.
- [107] L. Brown, J.K. Lanyi, *Proc. Natl. Acad. Sci. U. S. A.* 93 (1996) 1731–1734.
- [108] S. Subramaniam, T. Marti, H.G. Khorana, *Proc. Natl. Acad. Sci. U. S. A.* 87 (1990) 1013–1017.
- [109] H. Otto, T. Marti, M. Holz, T. Mogi, L.J. Stern, F. Engel, H.G. Khorana, M.P. Heyn, *Proc. Natl. Acad. Sci. U. S. A.* 87 (1990) 1018–1022.
- [110] S.P. Balashov, R. Govindjee, M. Kono, E. Imasheva, E. Lukashev, T.G. Ebrey, R.K. Crouch, D.R. Menick, Y. Feng, *Biochemistry* 32 (1993) 10331–10343.
- [111] E.S. Imasheva, S.P. Balashov, T.G. Ebrey, N. Chen, R.K. Crouch, D.R. Menick, *Biophys. J.* 77 (1999) 2750–2763.
- [112] M.S. Braiman, A.K. Dioumaev, J.R. Lewis, *Biophys. J.* 70 (1996) 939–947.
- [113] J. Heberle, D. Oesterhelt, N.A. Dencher, *EMBO J.* 12 (1993) 3721–3727.
- [114] K. Schulten, P. Tavan, *Nature* 272 (1978) 85–86.
- [115] T. Althaus, M. Stockburger, *Biochemistry* 37 (1998) 2807–2817.
- [116] H. Takei, Y. Gat, Z. Rothman, A. Lewis, M. Sheves, *J. Biol. Chem.* 269 (1994) 7387–7389.
- [117] H.J. Sass, R. Gessenich, M.H.J. Koch, D. Oesterhelt, N.A. Dencher, G. Büldt, F. Rapp, *Biophys. J.* 75 (1998) 399–405.
- [118] N.A. Dencher, J. Heberle, G. Büldt, H.-D. Höltje, M. Höltje, in: J.-L. Rigaud (Ed.), *Structure and Functions of Retinal Proteins*, John Libbey Eurotext, 1992, pp. 213–216.
- [119] S. Subramaniam, D.A. Greenhalgh, P. Rath, K.J. Rothschild, H.G. Khorana, *Proc. Natl. Acad. Sci. U. S. A.* 88 (1991) 6873–6877.
- [120] J.K. Delaney, U. Schweiger, S. Subramaniam, *Proc. Natl. Acad. Sci. U. S. A.* 92 (1995) 11120–11124.
- [121] J. Baudry, E. Tajkhorshid, R. Molnar, J. Phillips, K. Schulten, *J. Phys. Chem., B* 105 (2001) 905–918.
- [122] K. Murata, Y. Fujii, N. Enomoto, M. Hata, T. Hoshino, M. Tsuda, *Biophys. J.* 79 (2000) 982–991.
- [123] D. Oesterhelt, J. Tittor, E. Bamberg, *J. Bioenerg. Biomembranes* 24 (1992) 181–191.
- [124] S.P. Fodor, J.B. Ames, R. Gebhard, E.M. van der Berg, W. Stoekenius, J. Lugtenburg, R.A. Mathies, *Biochemistry* 27 (1988) 7097–7101.
- [125] S. Hayashi, I. Ohmine, *J. Phys. Chem., B* 104 (2000) 10678–10691.
- [126] W. Stoekenius, *Protein Sci.* 8 (1999) 447–459.
- [127] U. Haupts, J. Tittor, E. Bamberg, D. Oesterhelt, *Biochemistry* 36 (1997) 2–7.
- [128] L.S. Brown, A.K. Dioumaev, R. Needleman, J.K. Lanyi, *Biochemistry* 37 (1998) 3982–3993.
- [129] M. Wikström, *Curr. Opin. Struct. Biol.* 8 (1998) 480–488.
- [130] R.M. Esnouf, *J. Mol. Graph.* 15 (1997) 133–138.
- [131] E.A. Merritt, M.E. Murphy, *Acta Crystallogr., D* 50 (1994) 869–873.
- [132] N. Guex, M.C. Peitsch, *Electrophoresis* 18 (1997) 2714–2723.
- [133] T.A. Jones, J.-Y. Shou, S.W. Cowan, M. Kjeldgaard, *Acta Crystallogr., A* 47 (1991) 110–119.